Co-published by
Institute of Fluid-Flow Machinery
Polish Academy of Sciences
Committee on Thermodynamics and Combustion
Polish Academy of Sciences

http://www.imp.gda.pl/archives-of-thermodynamics/

Heat and Mass Transfer with Entropy Generation in Immiscible Fluid Flow through a Vertical Channel under Slip and Non-Uniform Thermal Conditions

Santhosh Kasula[a*], M.N. Raja Shekar[b]

[a]Sreyas Institute of Engineering and Technology, Hyderabad 500068, Telangana, India
[b]JNTUH University College of Engineering Science and Technology, Hyderabad 500068, Telangana, India
*Corresponding author email: kasula.santhosh54506@gmail.com

Received: 22.10.2025; revised: 19.12.2025; accepted: 04.01.2026

Abstract

The collective influence of slip and asymmetric heating is of great importance in many industries involving micro and macro-scale thermal systems, as it is directly related to flow resistance, thermal gradients and entropy generation. These effects are particularly relevant in channels with immiscible fluids, where wall fluid interactions and spatially varying boundary conditions govern the overall transfer behaviour. So the novelty of this work is a numerical analysis of entropy generation and heat and mass transfer in a vertical channel filled with two immiscible fluids, under a non-uniform heat, along with the influence of velocity slip. The system of governing equations of momentum, energy and diffusion is made non-dimensional using relevant variables, and then solved numerically using the Runge-Kutta method. The momentum, temperature and diffusion variations are presented in a graphical mode using data visualisation and smoothing via interpolation in Python for better visibility of the variations. The momentum, heat and mass transfer rates on both plates of the channel are also made non-dimensional. The other important parameter, entropy, is also calculated in the defined domain, and the obtained values are tabulated. The study found that all parameters, including slip effect, have a significant impact. In particular, the temperature, entropy generation and velocity are strongly affected by buoyancy forces and magnetic fields. The increase in Grashof number and molecular Grashof number improves fluid motion and reduces entropy. Both the increasing Reynolds number and magnetic parameter contribute to an increase in entropy generation. Shear stress analysis reveals two flow layers affected by buoyancy and magnetic damping.

Keywords: Heat and mass transfer; Non-uniform heat; Vertical channel; Entropy; Slip effects

Vol. 47(2026), No. 1, 177–194; doi: 10.24425/ather.2026.158668

Cite this manuscript as: Kasula, S., & Raja Shekar, M.N. (2026). Heat and Mass Transfer with Entropy Generation in Immiscible Fluid Flow through a Vertical Channel under Slip and Non-Uniform Thermal Conditions. *Archives of Thermodynamics*, 47(1), 177−194.

1. Introduction

Heat and mass transfer are fundamental processes that govern the movement of thermal energy and matter within physical systems. Heat flows due to temperature differences, while mass moves from high to low concentration regions. These mechanisms are vital in nature and industry, from climate systems to chemical reactors. Understanding them helps improve efficiency, reduce energy loss, and design better technologies. Fathima et al. [1] investigate the transfer of heat and mass in a two-layer viscous fluid flow affected by buoyancy motion. Profiles of temperature, velocity and concentration are acquired. Reddy et al. [2] explain the flow and heat transfer behaviour of fluids across an elongating surface under the influence of magnetic fields and thermal radiation. The results indicate that the fluid within the geometry exhibits a higher velocity. Srinivasulu and Goud [3] statistically analyse heat and mass transfer in Williamson nanofluid flow across a stretching surface with convective boundary conditions and an aligned magnetic field. Govindarajan et al. [4] analyse heat and mass transfer between two stratified immiscible fluids, focusing on interfacial oscillations and their impact on flow characteristics. They formulate equa-

Nomenclature

b_1, b_2 – thermal and solutal expansion ratios, $b_1 = \beta_{1T}/\beta_{2T}$, $b_2 = \beta_{1C}/\beta_{2C}$
B_0 – magnetic field strength, T
c_i – dimensionless concentration, $c_i = (C_i - C_*)/\Delta C$
C_i – concentration in fluid regions kg m^{-3}
C_*, C_L, C_R– reference and wall concentrations kg m^{-3}
D – mass diffusivity ratio, $D = D_1/D_2$
D_1, D_2 – mass diffusivities, m^2 s^{-1}
Du – Dufour number, Du = $D_1 \cdot K_{T1} \cdot \Delta C/(C_P \cdot C_{S1} \cdot \nu_1 \cdot \Delta T)$
Ec – Eckert number, Ec = $U_0^2/(C_{p1}\Delta T)$
g – acceleration due to gravity, m^2 s^{-1}
Gc – solutal Grashof number, Gc = $g \cdot \beta_{1C} \cdot \Delta C \cdot h_1^3/\nu_1^2$
Gr – thermal Grashof number, Gr = $g \cdot \beta_{1T} \cdot \Delta T \cdot h_1^3/\nu_1^2$
h – height ratio of the two fluid layers, $h = h_1/h_2$
h_1, h_2 – half widths of region 1 and region 2, m
k – micro polar fluid material parameter, $k = K/\mu_1$
K – vortex (spin) viscosity, Pa s
K_{T1}, K_{T2}–thermal conductivities, W m^{-1} K^{-1}
K_T – thermal conductivity ratio, $K_T = K_{T1}/K_{T2}$
m – dynamic viscosity ratio, $m = \mu_1/\mu_2$
M – magnetic interaction (Hartmann) parameter, $M = \sigma \cdot B_0^2 \cdot h_1^2/\mu_1$
n – dimensionless micro-rotation, $n = (h_1/u_0) \cdot N$
N – micro-rotation, s^{-1}
Pr – Prandtl number, Pr = ν_1/α_1
R – Reynolds number, $R = U_0 h_1/\nu_1$
Sc – Schmidt number, Sc = ν_1/D_1
Sr – Soret number, Sr = $D_1 \cdot K_{T1} \cdot \Delta T/(T_m \cdot D_1 \cdot \Delta C)$
T_i – fluid temperature, K
T_*, T_L, T_R–reference and wall temperatures, K
u_i – dimensionless axial velocity, $u_i = U_i/U_0$
U_0 – reference (mean) velocity, m s^{-1}
U_i – axial velocity in regions, m s^{-1}
y – dimensionless transverse coordinate in each region, $y = Y/h_i$
Y – transverse coordinate, m

Greek symbols

α – thermal conductivity ratio, $\alpha = k_1/k_2$
β – variable thermal conductivity parameter
β_{1T}, β_{2T}– thermal expansion coefficients, K^{-1}
β_{1C}, β_{2C}– solutal expansion coefficients, kg^{-1} m^{-3}
θ_i – dimensionless temperature $\theta_i = (T_i - T_*)/\Delta T$
θ_r – variable viscosity parameter
μ_1, μ_2 – dynamic viscosity, Pa s
$\mu\xi$ – dimensionless velocity slip parameter, $\mu\xi = \mu\xi^*/h_1$
$\mu\xi^*$ – dimensional velocity slip parameter, m
ρ_0 – reference density, kg m^{-3}
ρ_1, ρ_2 – fluid densities, kg m^{-3}
σ – electrical conductivity, S m^{-1}
ψ – dimensionless concentration ratio, $\psi = C_L/\Delta C$
ω, η – frequency parameters for thermal modulation, $\omega = \omega^*/h_1$, $\eta = \eta^*/h_2$
ω^*, η^* – dimensional frequency parameters, s^{-1}
Ω – dimensionless temperature ratio, $\Omega = T_L/\Delta T$

tions for mass, momentum, energy and concentration, examining parameters affecting the Nusselt and Sherwood numbers. Rabha and Deka [5] focus on heat and mass transfer in a porous medium with variable temperature and mass diffusion, specifically in the context of an accelerated plate. Nurni et al. [6] discuss heat and mass transfer in dynamic process systems, emphasising that simultaneous consideration of both transfers is essential, particularly during state transitions. Jan et al. [7] investigate the magnetohydrodynamic squeezing flow of an incompressible fluid through porous media exhibiting viscous dissipation, generated by converging parallel plates. The response surface methodology can help make important factors like magnetic strength, porosity and Eckert number better for predicting skin friction and heat transfer. Research helps to reduce drag and improve heat transfer in magnetohydrodynamic generators, extrusion processes and lubrication systems. Kumaraswamy et al. [8] consider internal heat sources, thermal conductivity, thermal slip and changing viscosity. They look at shear stress, Nusselt number, Sherwood number, temperature, diffusion profiles and velocity and angular velocity. The findings provide insights for engineering optimisation by highlighting the ways in which heat source intensity affects flow behaviour and transfer rates. Baithalu et al. [9] examine heat and mass transfer across an expanding surface within porous media, considering many effects. Based on their findings, using similarity transformations, the velocity and shear rate were diminished, whereas the fluid temperature rose with the increasing Eckert number.

Heat and mass transfer in a vertical channel involves the simultaneous flow of thermal energy and substances across vertical surfaces. This flow is driven by temperature and concentration differences. Natural convection and diffusion play a role in this process. It is essential in areas such as cooling systems, chemical processing and solar energy technologies. The interaction between thermal and solutal effects can either promote or hinder flow stability. Understanding these mechanisms is vital for the effective design and operation of engineering systems. Ouedraogo et al. [10] describe heat and mass transfer in a vertical channel under laminar forced convection, emphasising the significant impact of inlet fluid temperature on flow patterns and hydrodynamic fields, with latent heat transfer as the primary mode. Kalyan et al. [11] explore the heat and mass flow of two immiscible Jeffrey fluids within a vertical channel. Kemparaju et al. [12] investigate thermosolutal flow and heat mass transfer in a vertical porous annulus with localised vertical heating and insulated horizontals. In-line source-sink configurations optimise the circulation compared to alternatives; thermal mass dissipation is the highest through the upper source in counter-flow or through the lower inner source in other scenarios. A study by Baluguri et al. [13] offers a mathematical model for convective heat and mass transfer of two immiscible fluids in a vertically varying channel, considering diffusion-thermal effects and thermo-diffusion.

In a vertical channel with immiscible fluids, heat and mass transfer refers to the simultaneous motion of materials and thermal energy between two vertical surfaces that have two immiscible liquid layers. The interface between the fluids is essential, as variations in density, viscosity, thermal conductivity and diffusivity influence convection and diffusion processes. These systems are prevalent in applications like liquid heat exchangers, petroleum processing and environmental flows, where interfacial tension and buoyancy-driven motion govern the overall transfer properties. Comprehending these interconnected sys-

tems is crucial for enhancing performance and ensuring stability in both industrial and natural processes. The effects of Grashof numbers, viscosity ratio and heat generation on fluid flow and heat transfer are examined by Kandagal and Kempepatil [14] in their investigation of heat and mass transfer in vertical channels with immiscible fluid flow through a porous matrix. Kumar et al. [15] investigate the influence of radiation, Soret and Dufour effects on the laminar flow of a rotating fluid over a permeable plate amid chemical processes. The finite element method and similarity transformations are used to figure out the profiles of velocity, temperature and concentration. Gosty et al. [16] investigate heat and mass transfer in a vertical channel with immiscible fluids, focusing on slip effects. They analyse how variations in thermal conductivity and viscosity influence fluid dynamics, revealing significant interactions among slip mecha-nisms and engineering parameters like the Nusselt and Sherwood numbers. Srinivas et al. [17] explain heat and mass transfer in a vertical channel with immiscible fluids, focusing on variable viscosity and velocity slip. They reveal significant correlations affecting velocity, angular velocity, temperature and diffusion. Umavathi and Sheremet [18] analysed mixed convection in vertical channels, where a viscous fluid is sandwiched between nanofluids in a porous medium. The effects of the Grashof and Brinkman numbers, solid volume fraction and porous parameter on the velocity and temperature fields are investigated. Suresh et al. [19] investigate thermal slip's impact on heat and mass transfer in immiscible fluid flow within a vertical channel, highlighting that increased thermal slip decreases velocity and temperature profiles, while the Grashof and molecular Grashof numbers enhance fluid dynamics.

When two non-mixing liquids exchange thermal energy and species, heat and mass are transmitted along a vertical conduit filled with immiscible fluids, and entropy is created. This process is affected by interfacial phenomena and variations in characteristics. Entropy generation, arising from heat conduction, mass diffusion and viscous dissipation, quantifies irreversibility. It also enhances efficiency in thermal fluid systems. Naseem et al. [20] examine the generation of entropy in magnetohydrodynamic viscous flow across a permeable, radially extending disk, integrating Joule heating and radiative effects. Suction slows down the flow and heat transfer, while injection speeds them up. Magnetic fields reduce entropy near the disk, but their effects are weaker at greater distances.

Ghasemi and Ranjbar [21] numerically analyse entropy generation in a water-based alumina nanofluid flowing through vertical channels, considering the simultaneous effects of both forced and natural convection in a vertical channel with immiscible fluids. In a vertical channel with immiscible fluids, Suresh Babu et al. [22] explore heat and mass transmission, highlighting the impact of slip effects. They investigate the effects of viscosity and thermal conductivity variations on entropy generation, revealing complex interactions resulting from various thermal distributions and slip circumstances. Abdel et al. [23] investigate entropy generation in a micropolar fluid flowing through a corrugated channel, considering convective and slip boundary conditions. Mebarek-Oudina et al. [24] examine the magnetohydrodynamic flow of Burgers' fluid over a stretching cylinder, focusing on internal heat generation and absorption as well as temperature-dependent heat sources. Using similarity variables, the boundary layer equations are turned into ordinary differential equations. The BVP4C method is then used to find the velocity and temperature profiles.

In their study of entropy formation in the flow of a micropolar fluid via a vertical microchannel, Usha and Gireesha [25] took into consideration the combined effects of thermal radiation, viscous dissipation and Joule heating. In order to give a thorough grasp of the thermodynamic irreversibility in the system, the study additionally included convective boundary conditions. Kumar and Yadav [26] focus on analysing the entropy production characteristics of two non-miscible fluids, specifically couple stress and Newtonian fluids within an inclined porous channel. Govindarajulu et al. [27] investigate the entropy generation within a magnetohydrodynamic pulsatile flow of a third-grade hybrid nanofluid. The study focuses on the flow occurring between two vertical porous walls, considering several influencing factors, and analysing their effects on various physical quantities. Nayak et al. [28] conduct a computational analysis of the effects of the interfacial layer and shape on the Darcy-Forchheimer magnetohydrodynamic flow of single-walled and multi-walled carbon nanotube water nanofluids, including nonlinear thermal radiation and chemical processes. Enhanced nanoparticle form factors accelerate axial and radial flows while impeding tangential flow between disks, thereby affecting temperature, concentration, skin friction, Nusselt number, entropy and Bejan number profiles. Reddy et al. [29] investigate the complex behaviour of cross-flow fluid flow within microchannels, focusing on thermal and entropy generation aspects under specific conditions. The formation of entropy in the flow of Newtonian and immiscible micropolar fluids through a conduit was examined by Yadav et al. [30]. The investigation emphasised the impact of immiscibility of the micropolar and Newtonian viscous fluids on overall flow behaviour by looking at thermal properties, entropy production, flow velocity and Bejan number profiles. Prasad et al. [31] formulate a mathematical model for melting heat transmission in nanofluid flow using chemical processes and Joule heating. Complex nonlinear partial differential equations are simplified to ordinary differential equations by similarity transformations.

Khan et al. [32] explain Caputo fractional derivatives to elucidate memory effects in unsteady mixed convection within porous concentric cylinders. The temperature-dependent viscosity model is addressed by an implicit finite difference method, and the production of entropy from heat transfer, friction and porous resistance is analysed.

Shamshuddin and Ibrahim [33] examine the constant electromagnetohydrodynamic flow of a reactive Casson micropolar nanofluid between rotating parallel plates. The finite element method is employed to statistically resolve the issue while considering the influences of electric and magnetic forces. Madhuri et al. [34] examine heat transmission and nanofluid flow over a porous rotating disc influenced by buoyancy forces, incorporating thermal radiation effects via the Rosseland and Boussinesq approximations. Finite element study indicates that, although thermal radiation significantly influences temperature distribution, augmenting the volume fraction of nanoparticles enhances heat transfer efficiency. To optimise heat transmis-

sion, buoyancy forces alter flow topologies, impacting the thermal and velocity boundary layers.

Jan et al. [35] incorporate viscous dissipation and Ohmic heating while analysing boundary layer flow, thermal dynamics and hydrodynamic behaviour in battery systems utilising nanoparticles under cross non-Newtonian fluid conditions. Artificial neural networks in machine learning utilise numerical information to predict temperature distribution, heat transfer rates and energy efficiency, considering shear-thinning and thickening processes.

From the reviewed literature, it is observed that the present concept has not been previously addressed, i.e. entropy analysis in immiscible fluids in a vertical channel, considering the velocity slip. This study examines heat and mass transfer and entropy generation in a vertical channel containing immiscible fluids under non-uniform thermal distribution, considering the slip effect on the left wall. Entropy production, transfer rates and flow dynamics are all impacted by the interplay between fluid layers and temperature changes. To examine thermodynamic irreversibility and system performance, governing equations are solved. The findings demonstrate how important parameters affect the efficiency of heat and mass transfer. Entropy analysis sheds light on optimisation techniques and energy loss. The results help improve multi-fluid systems' thermal management.

2. Mathematical formulation

As shown in Fig. 1, the geometry is regarded as a vertical channel with two plates located at $Y = -h_1$ and $Y = h_2$ to investigate the entropy generation, heat and mass transfer in a vertical channel with immiscible fluids and non-uniform thermal distribution. The flow is thought to be fully formed. There are two regions in the channel: 0 to $-h_1$ and 0 to h_2. One of these regions is filled with micropolar fluid, while the other is filled with viscous fluid. Angular momentum characteristics are added to examine the nature of the system in the first region, which has micro-rotation. The system is assumed to satisfy the Boussinesq approximation.

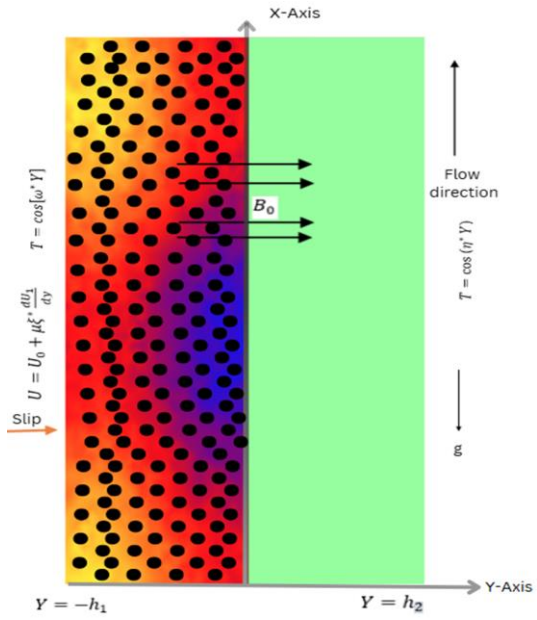

Fig. 1. Schematic diagram of the investigated system.

2.1. Governing equations

The governing equations for momentum, energy and species diffusion are derived based on the assumptions outlined in the mathematical formulation.

$$\frac{\partial U_1}{\partial Y} = 0, \frac{\partial U_2}{\partial Y} = 0, \tag{1}$$

$$\rho_1 = \rho_0[1 - \beta_{1T}(T_1 - T_*) - \beta_{1C}(C_1 - C_*)],$$

$$\rho_2 = \rho_0[1 - \beta_{2T}(T_2 - T_*) - \beta_{2C}(C_2 - C_*)], \tag{2}$$

$$\left(\mu_1 + \frac{K}{2}\right) {h_1}^2 \frac{\partial^2 N}{\partial Y^2} - K\left(2N + \frac{\partial U_1}{\partial Y}\right) = 0, \tag{3}$$

$$\frac{1}{\rho_1}\frac{\partial}{\partial Y}(\mu_1 + K)\frac{\partial U_1}{\partial Y} + \frac{K}{\rho_1}\frac{\partial N}{\partial Y} + g\beta_{1T}(T_1 - T_*) +$$

$$+ g\beta_{1C}(C_1 - C_*) - \sigma\frac{B_0^2 U_1}{\rho_1} = 0, \tag{4}$$

$$\frac{1}{\rho_2}\frac{\partial}{\partial Y}\left(\mu_2\frac{\partial U_2}{\partial Y}\right) + g\beta_{2T}(T_2 - T_*) +$$

$$+ g\beta_{2c}(C_2 - C_*) - \sigma\frac{B_0^2 U_2}{\rho_2} = 0, \tag{5}$$

$$\frac{\partial}{\partial Y}(K_{T1}\frac{\partial T_1}{\partial Y}) + \mu_1\left(\frac{\partial U_1}{\partial Y}\right)^2 + \frac{\rho_1 D_1 K_{T1}}{C_{s1}}\frac{\partial^2 C_1}{\partial Y^2} = 0, \tag{6}$$

$$\frac{\partial}{\partial Y}(K_{T2}\frac{\partial T_2}{\partial Y}) + \mu_2\left(\frac{\partial U_2}{\partial Y}\right)^2 + \frac{\rho_2 D_2 K_{T2}}{C_{s2}}\frac{\partial^2 C_2}{\partial Y^2} = 0, \tag{7}$$

$$D_1\frac{\partial^2 C_1}{\partial Y^2} + \frac{D_1 K T_1}{T_m}\frac{\partial^2 T_1}{\partial Y^2} = 0, \tag{8}$$

$$D_2\frac{\partial^2 C_2}{\partial Y^2} + \frac{D_2 K_{T2}}{T_m}\frac{\partial^2 T_2}{\partial Y^2} = 0. \tag{9}$$

2.2. Entropy generation

The dimensional entropy production for the current problem is derived as given by Bejan [36]:

$$E_{gen} = E1_{gen} + E2_{gen} \tag{10}$$

where:

$$E1_{gen} = \frac{1}{h_1 T_L}\int_{-h_1}^{0}[\mu_1 + K]\left(\frac{dU_1}{dY}\right)^2 dY +$$

$$+ \frac{1}{{h_1}{T_L}^2}\int_{-h_1}^{0} K_{T_1}\left(\frac{dT_1}{dY}\right)^2 dY + \frac{1}{h_1}\int_{-h_1}^{0}\frac{\sigma {B_0}^2 {U_1}^2}{T_L} dY +$$

$$+ \frac{1}{{C_L}^2 h_1}\int_{-h_1}^{0} D_1\left(\frac{dC_1}{dY}\right)^2 dY,$$

$$E2_{gen} = \frac{1}{h_2 T_R}\int_{0}^{h_2}\mu_2\left(\frac{dU_2}{dY}\right)^2 dY + \frac{1}{{h_2}{T_R}^2}\int_{0}^{h_2} K_{T_2}\left(\frac{dT_2}{dY}\right)^2 dY +$$

$$+ \frac{1}{h_2}\int_{0}^{h_2}\frac{\sigma {B_0}^2 {U_2}^2}{T_R} dY + \frac{1}{{C_R}^2 h_2}\int_{0}^{h_2} D_2\left(\frac{dC_2}{dY}\right)^2 dY.$$

2.3. Boundary and interface conditions

The flow domain consists of two immiscible fluid layers confined between two vertical plates separated by a total width of $h_1 + h_2$. The left wall $Y = -h_1$ is maintained at a prescribed oscillatory temperature distribution, and allows velocity slip and

thermal modulation. At the interface $Y = 0$, both the velocity and the stress are continuous, as are the temperature, heat flux, concentration and mass flux. The right wall $Y = h_2$ is also maintained with thermal modulation controlled by another parameter.

2.3.1. Dimensional form

At $Y = -h_1$ we have:

$$U = U_0 + \mu\xi^* \frac{dU_1}{dy}, \quad T = \cos(\omega^* Y), \quad C = C_*, \quad N = 0. \quad (11a)$$

At $Y = 0$:

$$U_1 = U_2, \quad \frac{dN}{dY} = 0, \quad T_1 = T_2, \quad C_1 = C_2, \quad \mu_1 \frac{dU_1}{dY} = \mu_2 \frac{dU_2}{dY},$$
$$k_{T1} \frac{dT_1}{dY} = k_{T2} \frac{dT_2}{dY}, \quad D_1 \frac{dC_1}{dY} = D_2 \frac{dC_2}{dY}. \quad (11b)$$

At $Y = h_2$:

$$U = 0, \qquad T = \cos(\eta^* Y), \qquad C = C_*. \quad (11c)$$

2.3.2. Non-dimensional form

At $y = -1$ we have:

$$u_1 = 1 + \mu\xi \frac{du_1}{dy}, \quad \theta_1 = \cos(\omega y), \quad n = 0, \quad c_1 = 1. \quad (12a)$$

At $y = 0$:

$$u_1 = u_2, \quad \frac{dn}{dy} = 0, \quad \theta_1 = \theta_2, \quad c_1 = c_2, \quad \frac{du_2}{dy} = mh \frac{du_1}{dy},$$
$$\frac{d\theta_2}{dy} = h\,\alpha \frac{d\theta_1}{dy}, \quad \frac{dc_2}{dy} = Df \frac{dc_1}{dy}. \quad (12b)$$

At $y = 1$:

$$u_2 = 0, \qquad \theta_2 = \cos(\eta y), \qquad c_2 = 0. \quad (12c)$$

2.3.3. Physical interpretation

The boundary condition on the right wall incorporates a velocity slip effect governed by the dimensionless parameter $\mu\xi$. For $\mu\xi = 0$, the surface behaves as a classical no-slip wall, whereas increasing $\mu\xi > 0$ allows partial fluid slippage, accounting for rarefaction effects, micro layer formation, or surface coatings that reduce shear resistance. The temperature at each wall varies periodically with Y to simulate thermal oscillations or uneven wall heating. At the fluid interface ($y = 0$), continuity of velocity, temperature and concentration ensures smooth transfer of momentum, heat and mass between the two immiscible layers, while equality of their respective fluxes ensures conservation across the interface.

2.4. Non-dimensional system

The governing equations and the respective boundary conditions are converted into non-dimensional forms as follows, which are given in region 1 and region 2:

$$\frac{d^2 n}{dy^2} - \frac{2k}{2+k}\left(2n + \frac{du_1}{dy}\right) = 0, \quad (13)$$

$$k\frac{dn}{dy} + \frac{\theta_r}{(\theta_1-\theta_r)^2}\frac{d\theta_1}{dy}\frac{du_1}{dy} - \frac{\theta_r}{\theta_1-\theta_r}\frac{d^2u_1}{dy^2} + $$
$$+\frac{\mathrm{Gr}}{\mathrm{R}}\theta_1 + \frac{\mathrm{Gc}}{\mathrm{R}}c_1 - Mu_1 = 0, \quad (14)$$

$$\beta\left(\frac{d\theta_1}{dy}\right)^2 + (1+\beta\theta_1)\frac{d^2\theta_1}{dy^2} - \mathrm{PrEc}\frac{\theta_r}{\theta_1-\theta_r}\left(\frac{du_1}{dy}\right)^2 + \mathrm{Du}\frac{d^2c_1}{dy^2} = 0, \quad (15)$$

$$\frac{1}{\mathrm{Sc{\cdot}R}}\frac{d^2c_1}{dy^2} + \mathrm{Sr}\frac{d^2\theta_1}{dy^2} = 0, \quad (16)$$

$$\frac{\theta_r}{(\theta_2-\theta_r)^2}\frac{d\theta_2}{dy}\frac{du_2}{dy} - \frac{\theta_r}{(\theta_2-\theta_r)}\frac{d^2u_2}{dy^2} + \frac{1}{a{\cdot}b{\cdot}f^2}\frac{\mathrm{Gr}}{\mathrm{R}}\theta_2 + $$
$$+\frac{1}{a{\cdot}b{\cdot}f^2}\frac{\mathrm{Gc}}{\mathrm{R}}c_2 - Mu_2 = 0, \quad (17)$$

$$\beta\left(\frac{d\theta_2}{dy}\right)^2 + (1+\beta\theta_2)\frac{d^2\theta_2}{dy^2} - a\,\mathrm{Pr\,Ec}\left(\frac{\theta_r}{\theta_2-\theta_r}\right)\left(\frac{du_2}{dy}\right)^2 +$$
$$+\mathrm{Du}\frac{d^2c_2}{dy^2} = 0, \quad (18)$$

$$\frac{f}{d\,\mathrm{Sc\,R}}\frac{d^2c_2}{dy^2} + \frac{f{\cdot}\mathrm{Sr}}{K_T{\cdot}d}\frac{d^2\theta_2}{dy^2} = 0. \quad (19)$$

The non-dimensional transfer rates on the boundaries using the non-dimensional variables are obtained as:

– shear stress on the channel's left plate:

$$st_1 = \left[\frac{du_1}{dy}\right]_{y=-1}, \quad (20a)$$

– shear stress on the channel's right plate:

$$st_2 = \left[\frac{du_2}{dy}\right]_{y=1}, \quad (20b)$$

– Nusselt number on the channel's left plate:

$$\mathrm{Nu}_1 = \left[\frac{d\theta_1}{dy}\right]_{y=-1}, \quad (20c)$$

– Nusselt number for the channel's right plate:

$$\mathrm{Nu}_2 = \left[\frac{d\theta_2}{dy}\right]_{y=1}, \quad (20d)$$

– Sherwood number on the channel's left plate:

$$\mathrm{Sh}_1 = \left[\frac{dc_1}{dy}\right]_{y=-1}, \quad (20e)$$

– Sherwood number on the channel's right plate:

$$\mathrm{Sh}_2 = \left[\frac{dc_2}{dy}\right]_{y=1}. \quad (20f)$$

Entropy in the considered domain is obtained in the non-dimensional form as:

$$e_{gen} = e1_{gen} + e2_{gen}, \quad (21)$$

where:

$$e1_{gen} = \mathrm{PrEc}\int_{-1}^{0}\left[\frac{\theta_r - k(\theta_1-\theta_r)}{\theta_1-\theta_r}\left(\frac{du_1}{dy}\right)^2\right]dy +$$
$$+\frac{1}{\Omega}\int_{-1}^{0}\left[(1+\beta\theta_1)\left(\frac{d\theta_1}{dy}\right)^2\right]dy + \frac{1}{\mathrm{Sc}\,\psi^2}\int_{-1}^{0}\left(\frac{dc_1}{dy}\right)^2 dy +$$
$$+M{\cdot}\mathrm{Pr}{\cdot}\mathrm{Ec}\int_{-1}^{0}({u_1}^2)\,dy,$$

$$e2_{gen} = \frac{h\,\mathrm{PrEc}\,\alpha}{m}\int_0^1 [(\frac{\theta_r - k(\theta_2 - \theta_r)}{\theta_2 - \theta_r})\left(\frac{du_2}{dy}\right)^2]\,dy +$$

$$+\frac{h}{\Omega}\int_0^1 [(1+\beta\,\theta_2)\left(\frac{d\theta_2}{dy}\right)^2]\,dy + \frac{d}{\mathrm{Sc}\psi^2}\int_0^1 \left(\frac{dc_2}{dy}\right)^2 dy +$$

$$+\frac{MPr\mathrm{Ec}\,\alpha}{h}\int_0^1 (u_2{}^2)\,dy.$$

3. Solution of the problem

The non-dimensional system of Eqs. (13) to (19), subjected to boundary conditions Eqs. (12a−12c), are solved using the Mathematica package under the ND Solve technique. Using an integrated shooting strategy, the boundary value problem will be transformed into an initial value problem. The required coefficients will then be computed until the required precision of 10^{-5} is achieved. The method's convergence is confirmed by meeting the boundary requirements. Utilising the formulas found in Eqs. (20a−20f), the rates of mass and heat transmission are determined. The entropy is also calculated from the obtained non-dimensional Eq. (21). All the governing parameter values are considered in possible combinations to analyse the variations in the form of graphs.

4. Results and discussion

The effects of important physical factors, such as the Grashof number (Gr), molecular Grashof number (Gc), magnetic field parameter (M), Reynolds number (R), material parameter (k), variable viscosity parameter (θ_r), velocity slip parameter ($\mu\zeta$), Soret number (Sr), Schmidt number (Sc), dimensionless temperature ratio (Ω), dimensionless concentration ratio (ψ), Eckert number (Ec), Dufour number (Du), variable thermal conductivity (β) and frequency parameters (ω, η) were carefully examined and presented in graphical mode using data visualisation and smoothing via interpolation in Python for better visibility of the variations.

4.1. Analysis of velocity, angular velocity, temperature, and concentration

Figures 2−7 depict the variations of velocity with respect to Grashof number (Gr), molecular Grashof number (Gc), magnetic field (M), Reynolds number (R), material parameter (k) and velocity slip parameter ($\mu\zeta$). The increase in molecular Grashof number (Gc) provides a modest enhancement in velocity due to mass transfer effects, but elevated Grashof numbers (Gr) and material parameters (k) significantly enhance the flow by augmenting buoyancy forces and favourable material characteris-

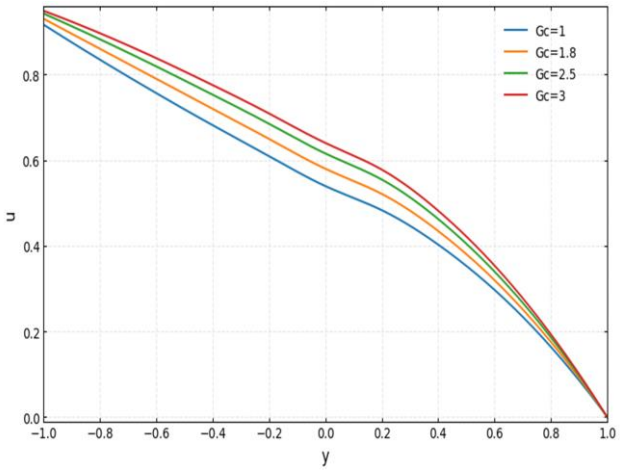

Fig. 3. Change of velocity with respect to molecular Grashof number (Gc).

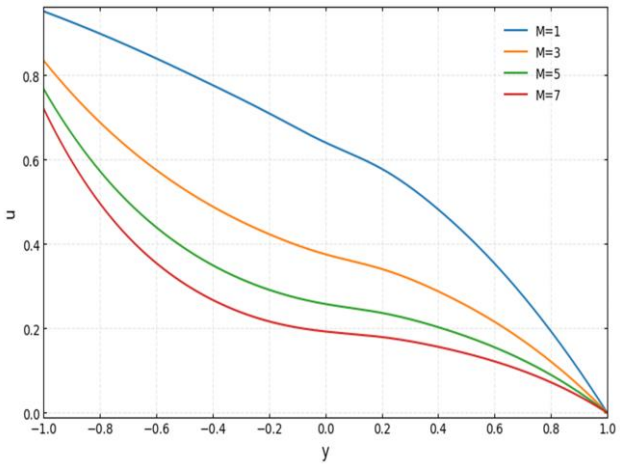

Fig. 4. Change of velocity with respect to the magnetic field (M).

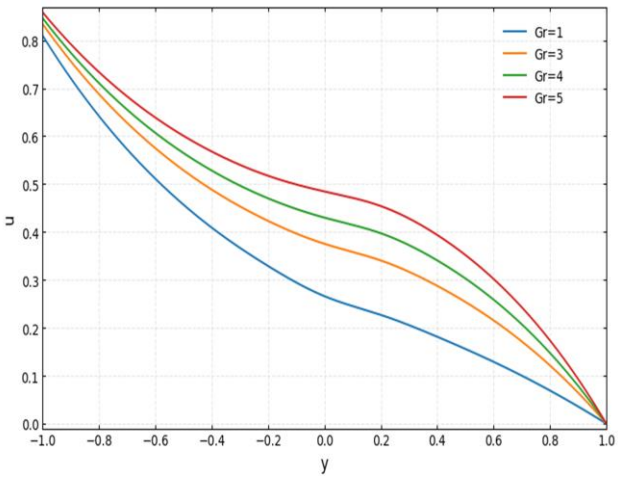

Fig. 2. Change of velocity with respect to Grashof number (Gr).

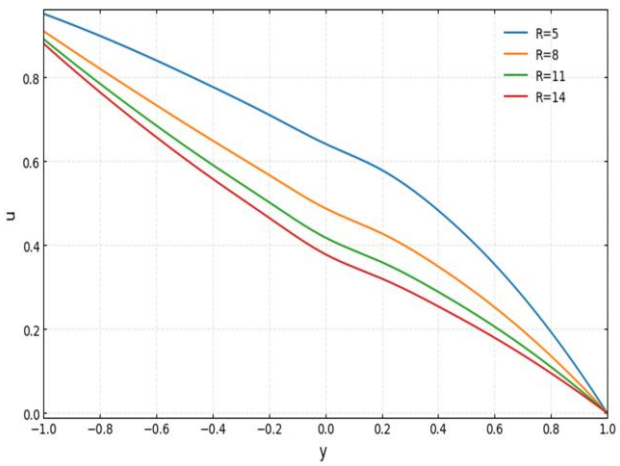

Fig. 5. Change of velocity with respect to Reynolds number (R).

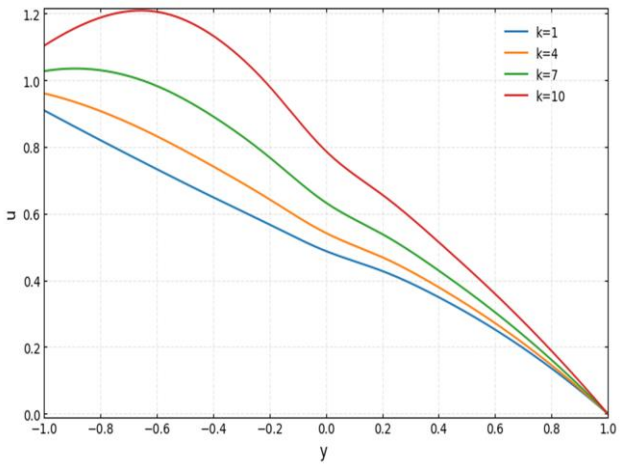

Fig. 6. Change of velocity with respect to the material parameter (k).

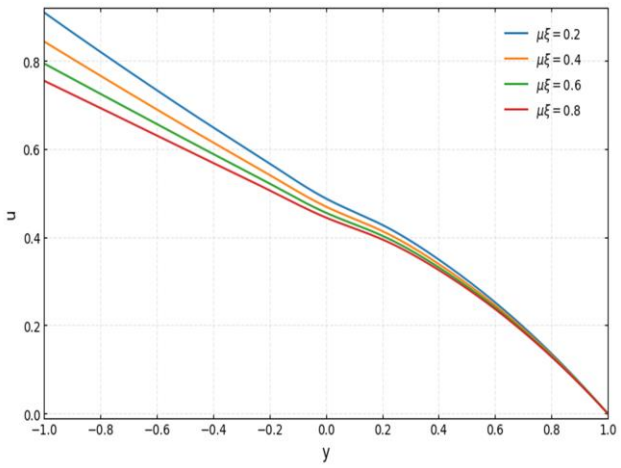

Fig. 7. Change of velocity with respect to the velocity slip parameter ($\mu\xi$).

tics. The effect of buoyancy forces is significant on both thermal and solutal Grashof numbers. Conversely, inertial forces tend to resist the flow. The presence of a magnetic field further suppresses the velocity due to the Lorentz force. Consequently, an increase in the Reynolds number (R) and magnetic parameter (M) leads to a marked reduction in velocity. However, the velocity slip parameter ($\mu\xi$) exhibits comparatively weaker damping, while higher viscosity increases flow resistance under slip conditions.

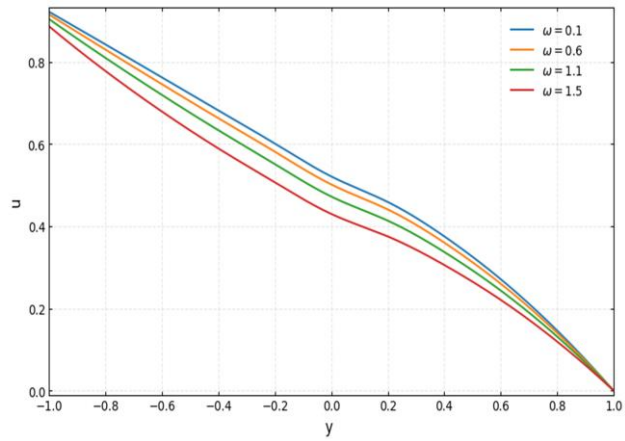

Fig. 8. Change of velocity with respect to frequency parameter (ω).

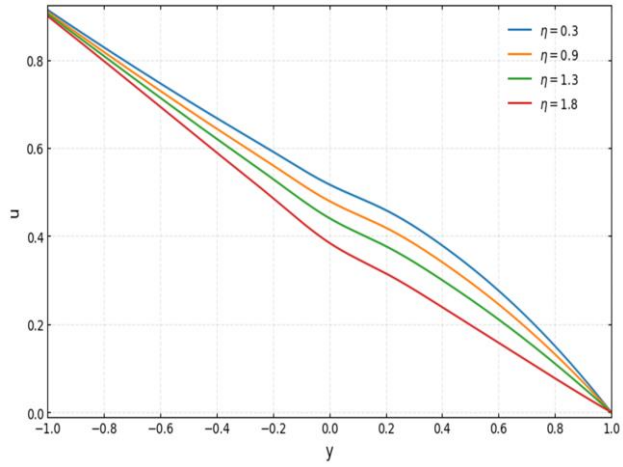

Fig. 9. Change of velocity with respect to frequency parameter (η).

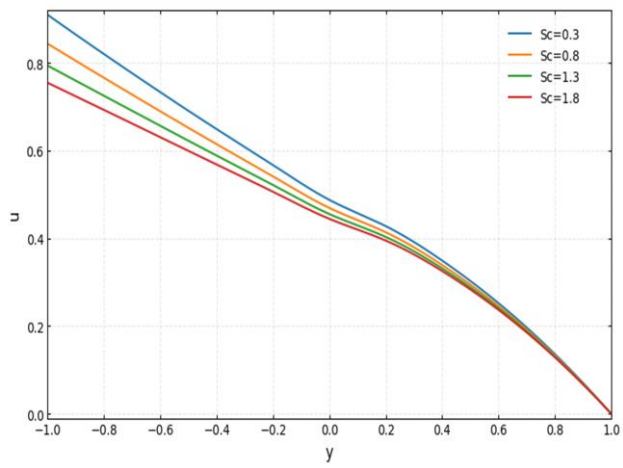

Fig. 10. Change of velocity with respect to Schmidt number (Sc).

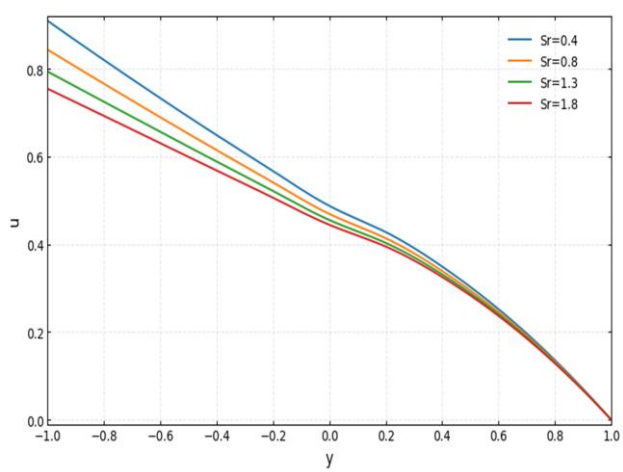

Fig. 11. Change of velocity with respect to Soret number (Sr).

In Figs. 8–13, it is demonstrated that when any of the parameters like frequency parameters (η, ω), Schmidt number (Sc),

Soret number (Sr), dimensionless temperature ratio (Ω) and dimensionless concentration ratio (ψ) increases, then a decrease in velocity is observed across the whole domain.

Since the increased viscosity decreases the mobility of fluids, this reduction becomes more apparent with the increasing values of frequency. This is due to oscillatory or time-dependent forcing effects on the fluid. Simultaneously, additional variables reduce velocity by increasing the mass diffusivity, altering heat diffusion, and quickening the rates of concentration. This effect is due to the increased momentum diffusivity to mass diffusivity ratio. Also, the thermophoresis effect on velocity is significant. So, upon the variation of the Soret number, these pertinent parameters vary. The dimensionless temperature ratio represents the relative temperature difference between the channel walls or fluid layers, and the dimensionless concentration ratio reflects the relative concentration difference between the plates or fluid layers. Since the non-uniform heating is applied, these effects are significant.

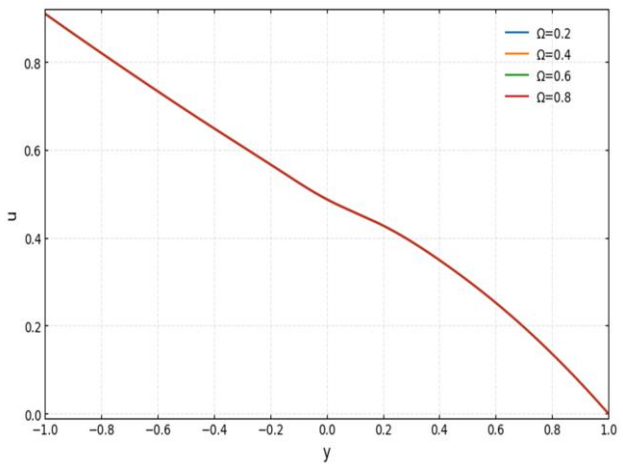

Fig. 12. Change of velocity with respect to dimensionless temperature ratio (Ω).

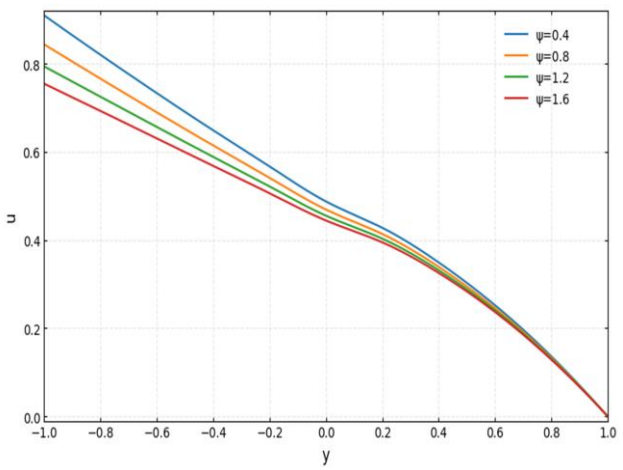

Fig. 13. Change of velocity with respect to dimensionless concentration ratio (ψ).

The temperature profiles (Figs. 14–19) illustrate the different effects of various parameters on the thermal behaviour of the fluid. Increased buoyant forces that enhance heat transfer result in a small temperature increase in the core region as the Grashof number (Gr) escalates. Magnetic damping reduces the velocity and allows for more heat accumulation, leading to a gradual yet consistent increase in temperature with a higher magnetic field value (M). Elevated Reynolds numbers (R) signify poorer convective cooling at reduced velocities, resulting in increased temperatures. As the material parameter (k) increases, the tempera-

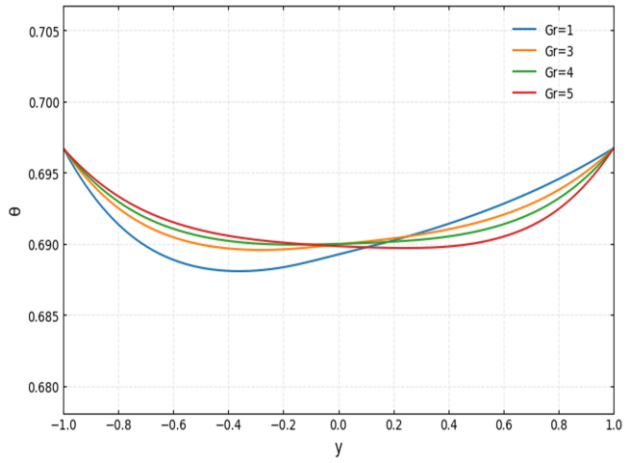

Fig. 14. Change of temperature with respect to Grashof number (Gr).

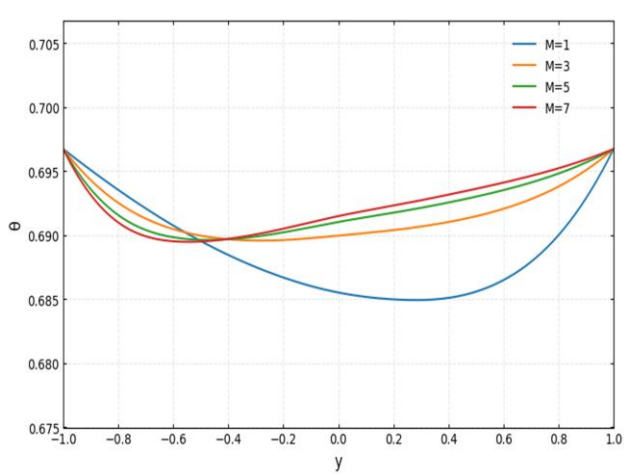

Fig. 15. Change of temperature with respect to magnetic field (M).

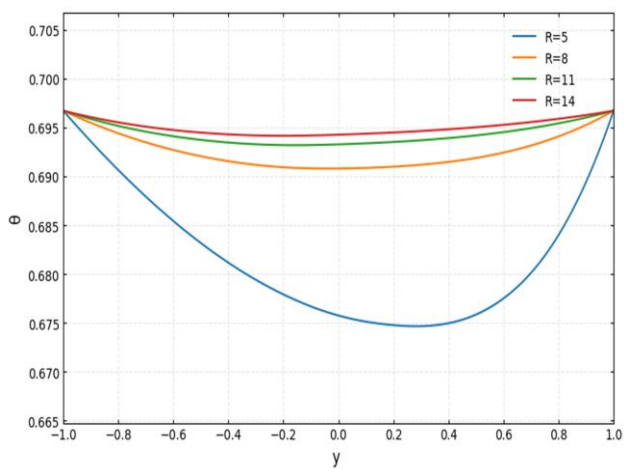

Fig. 16. Change of temperature with respect to Reynolds number (R).

ture decreases, indicating enhanced thermal conductivity that facilitates heat dissipation.

An increase in the variable viscosity parameter (θ_r) leads to a slight rise in temperature, indicating additional heat generation within the system. As the Eckert number (Ec) rises, the temperature profile diminishes, indicating heightened viscous dissipation effects that facilitate localised cooling in the core and convert kinetic energy into thermal energy. The temperature increases with factors that enhance heat retention, whereas its distribution is significantly influenced by mechanisms that promote heat loss or induce thermal fluctuations.

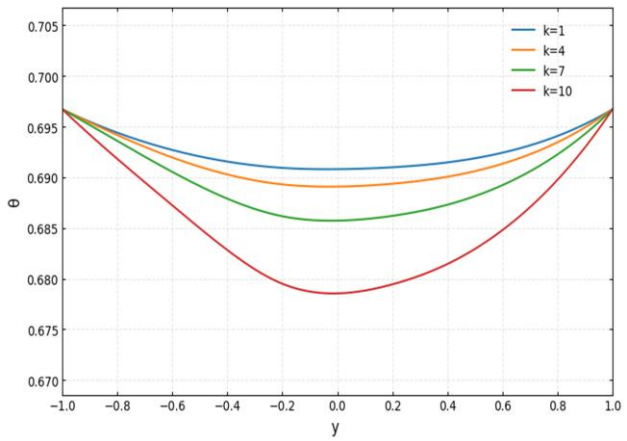

Fig. 17. Change of temperature with respect to material parameter (k).

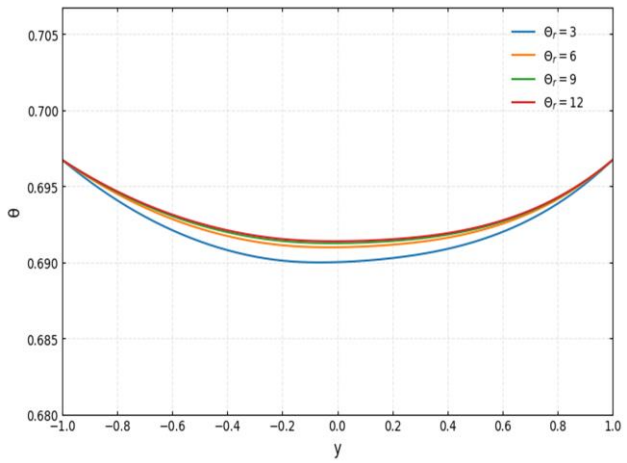

Fig. 18. Change of temperature with respect to viscosity parameter (θ_r).

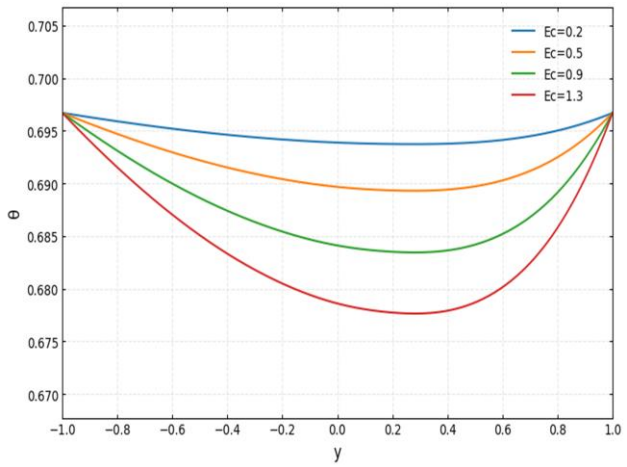

Fig. 19. Change of temperature with respect to Eckert number (Ec).

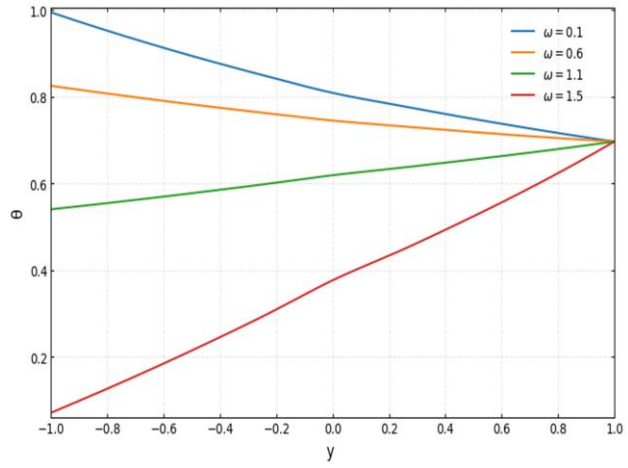

Fig. 20. Change of temperature with respect to non-uniform temperature amplitude (ω).

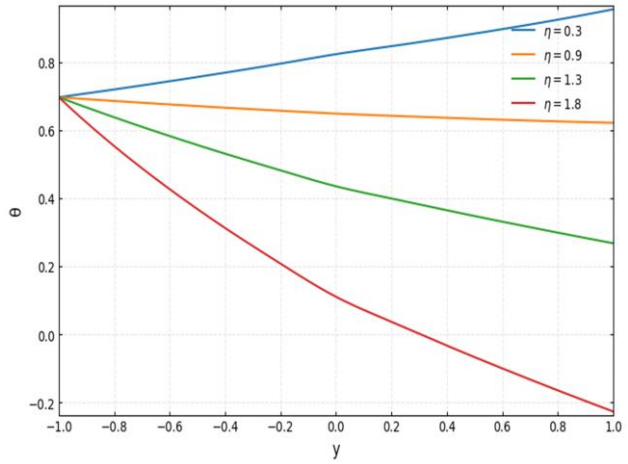

Fig. 21. Change of temperature with respect to non-uniform temperature amplitude (η).

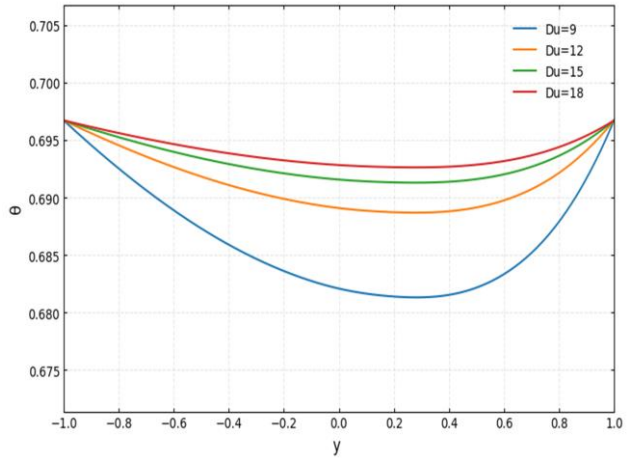

Fig. 22. Change of temperature with respect to Dufour number (Du).

The impact of different parameters on the thermal behaviour of the system is depicted in the temperature profiles in Figs. 20−28. The temperature profile is significantly influenced by the frequency parameter (ω). Elevated values markedly alter the distribution and slope, signifying pronounced thermal oscillations. The temperature distribution is significantly influenced by an increase in the frequency parameter (η), since elevated η markedly reduces the temperature in certain areas of the domain due to increased thermal non-uniformity. The significance of thermal mass diffusion coupling is further underscored by the observation that an increased Dufour number (Du) results in a temperature decrease at the centre, and in a small increase towards the walls. The minimal variation in the Schmidt number (Sc) and Soret number (Sr) indicates that mass diffusivity and thermodiffusion exert a diminished influence on temperature.

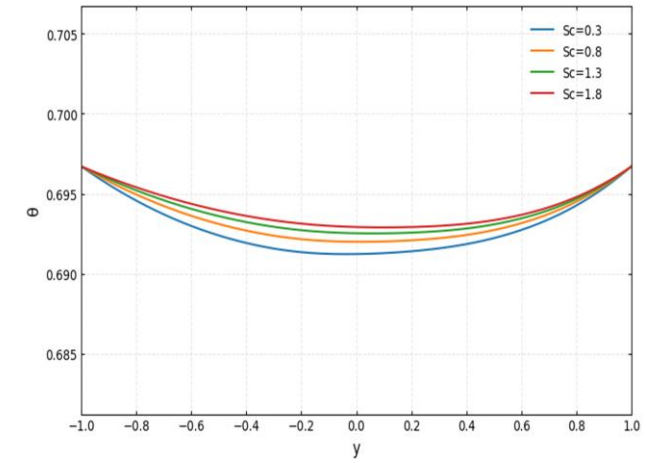

Fig. 23. Change of temperature with respect to Schmidt number (Sc).

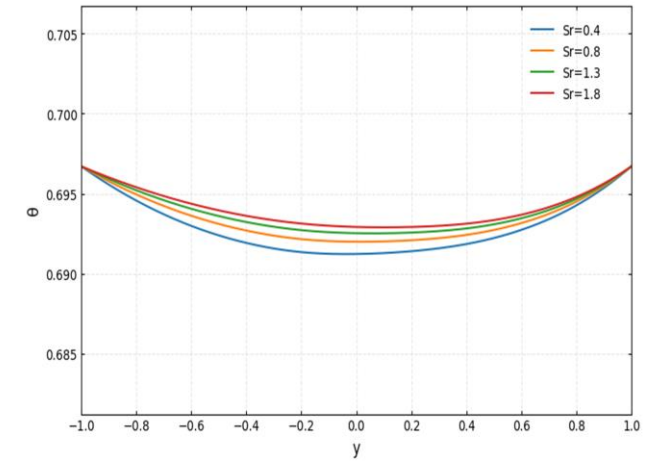

Fig. 24. Change of temperature with respect to Soret number (Sr).

As it ascends, variable thermal conductivity (β) diminishes the temperature, signifying enhanced thermal conduction or related physical resistance. An increase in the velocity slip parameter $\mu\xi$ causes a small increase in the temperature profile, which then becomes more uniform throughout the entire region. More slip at the wall reduces thermal gradients, leading to a more uniform distribution of temperature. Different values of the dimensionless temperature ratio (Ω) are shown by different temperature profiles (Ω), which are almost the same and do not change much as Ω goes up. Finally, for elevated values, the dimensionless concentration ratio (ψ) increases the temperature marginally, presumably due to contributions from exothermic reactions.

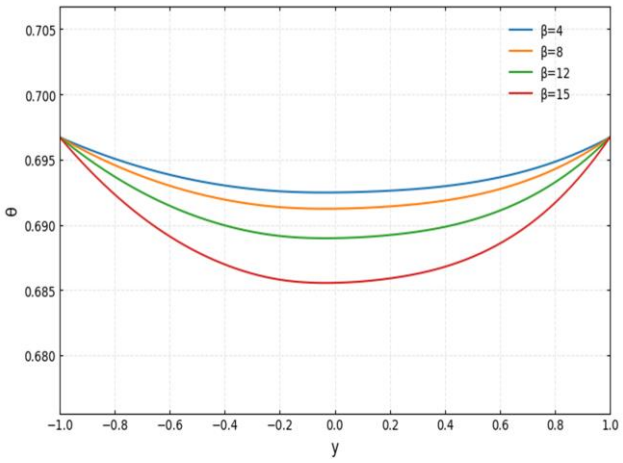

Fig. 25. Change of temperature with respect to variable thermal conductivity (β).

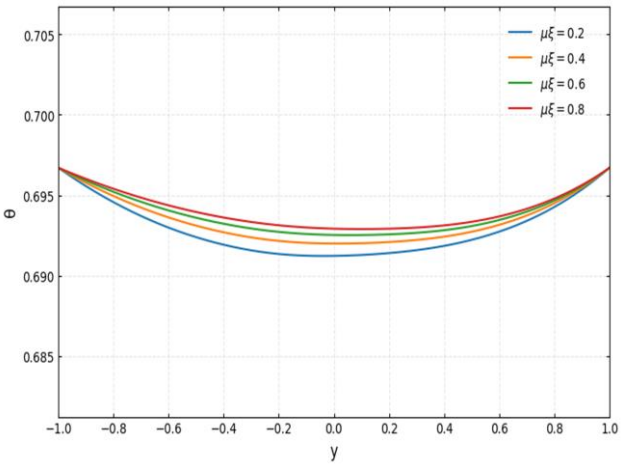

Fig. 26. Change of temperature with respect to the velocity slip parameter ($\mu\xi$).

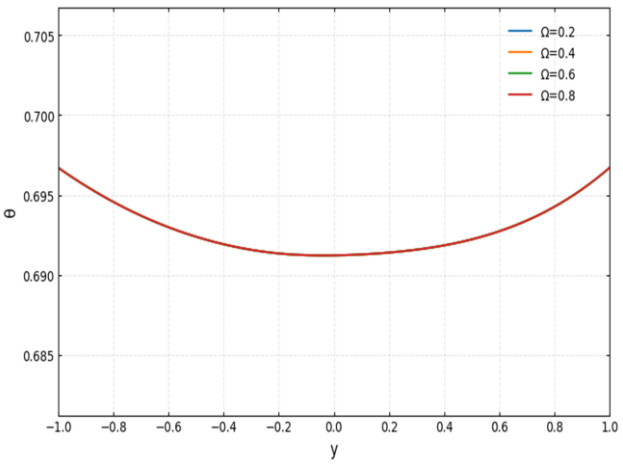

Fig. 27. Change of temperature with respect to the dimensionless temperature ratio (Ω).

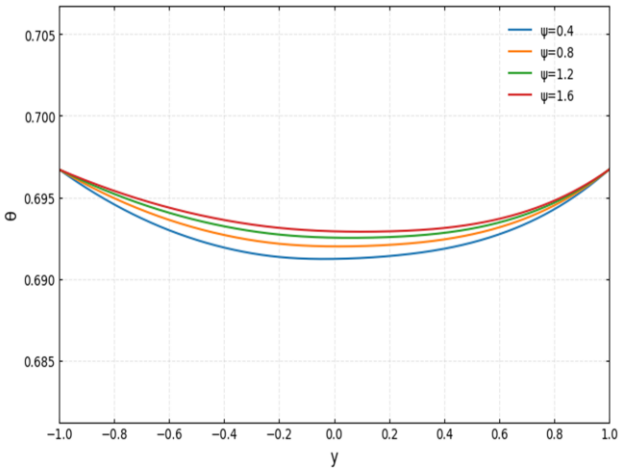

Fig. 28. Change of temperature with respect to dimensionless concentration ratio (ψ).

The angular momentum profiles in Figs. 29–38 show that different parameters have varying effects on the distribution of momentum. The angular momentum is increased throughout the domain by increasing the Reynolds number (R) and the magnetic field parameter (M). The effect is more significant for greater M due to the influence of magnetic forces on rotational flow, and for bigger R because of the augmented inertial effects. Beneficial material qualities enhance rotational motion, as demonstrated by the significant positive impact of the material parameter (k), with the angular momentum markedly increasing for elevated values of k. The variable viscosity parameter (θ_r) leads to a minor enhancement in angular momentum, suggesting that alterations in viscosity slightly affect rotational characteristics. The angular momentum experiences a minor rise with an elevation in the frequency parameter ω, whereas the frequency parameter η exerts a more pronounced positive influence, perhaps due to enhanced thermal gradients that facilitate rotational motion. When the dimensionless temperature ratio (Ω) increases, the value of angular momentum rises gradually, but the overall change remains very small. This shows that varying Ω has only a minor effect on angular momentum within the domain.

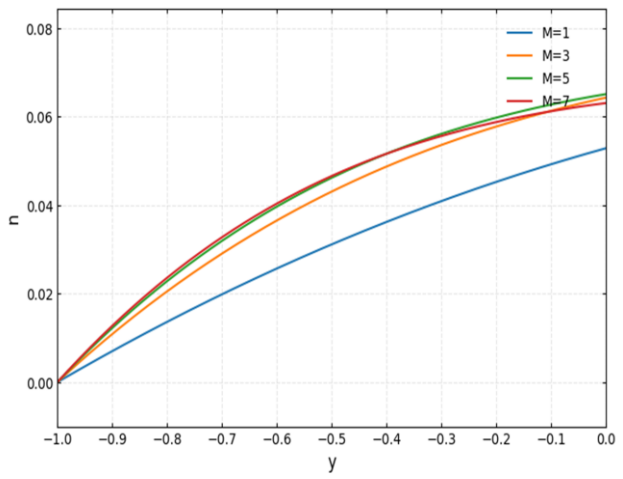

Fig. 29. Change of angular momentum with respect to magnetic field (M).

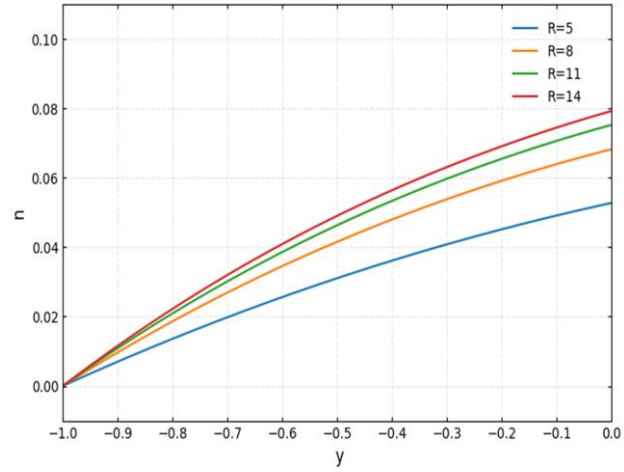

Fig. 30. Change of angular momentum with respect to Reynolds number (R).

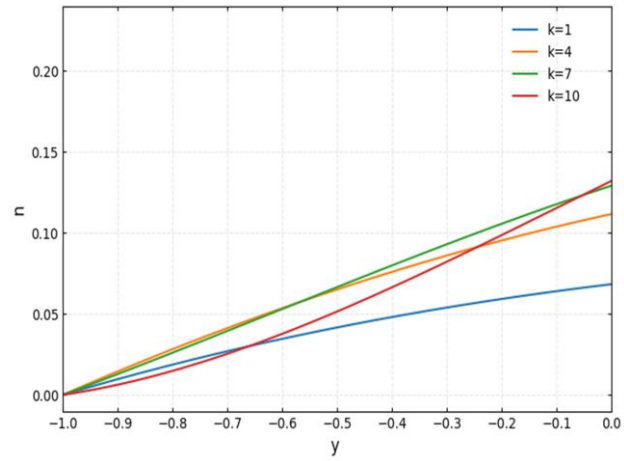

Fig. 31. Change of angular momentum with respect to material parameter (k).

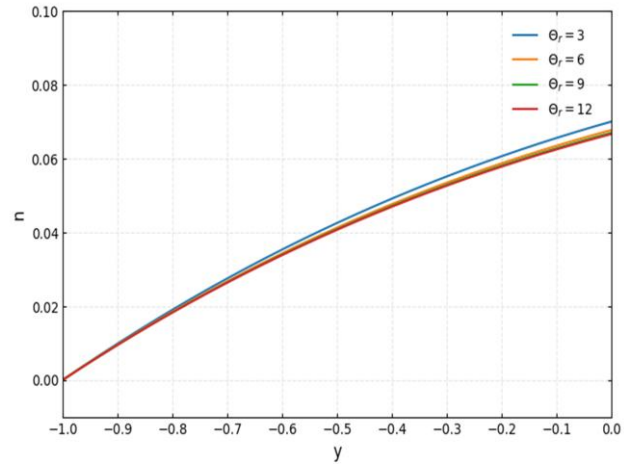

Fig. 32. Change of angular momentum with respect to viscosity parameter (θ_r).

A higher Schmidt number (Sc), dimensionless concentration ratio (ψ) and velocity slip parameter ($\mu\xi$) collectively diminish the angular momentum, indicating that the enhanced resistance

to mass diffusivity, reaction rates, and viscosity effects hinder rotational flow.

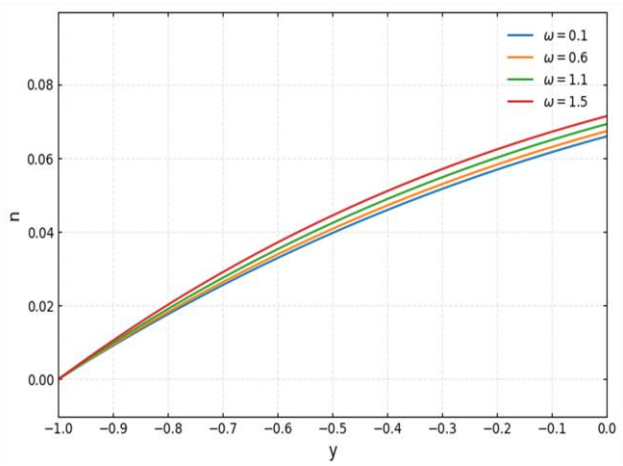

Fig. 33. Change of angular momentum with respect to non-uniform temperature amplitude (ω).

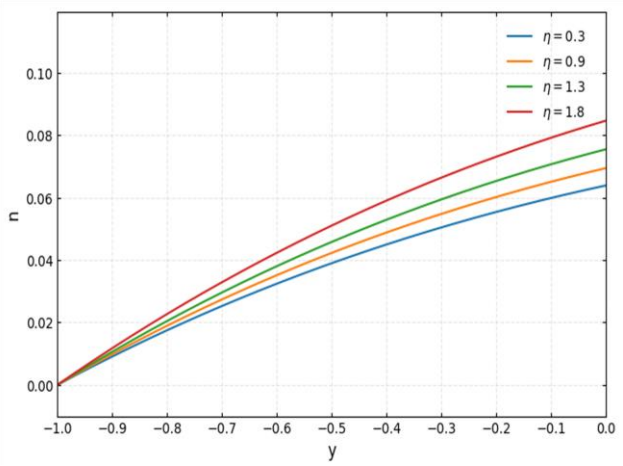

Fig. 34. Change of angular momentum with respect to non-uniform temperature amplitude (η).

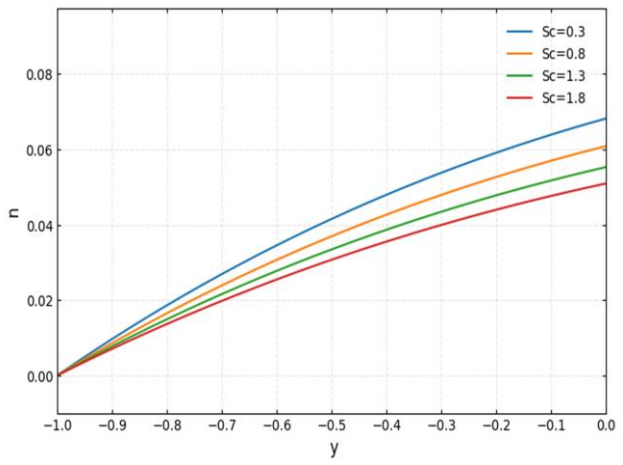

Fig. 35. Change of angular momentum with respect to Schmidt number (Sc).

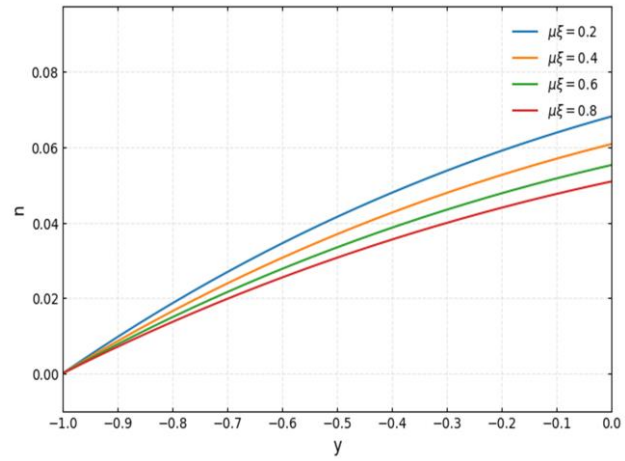

Fig. 36. Change of angular momentum with respect to the velocity slip parameter ($\mu\zeta$).

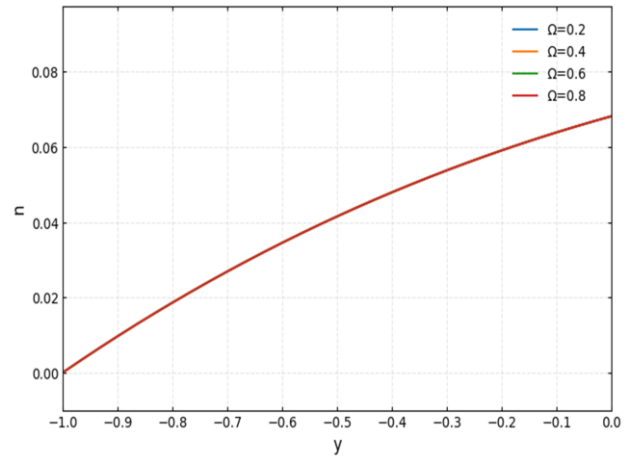

Fig. 37. Change of angular momentum with respect to dimensionless temperature ratio (Ω).

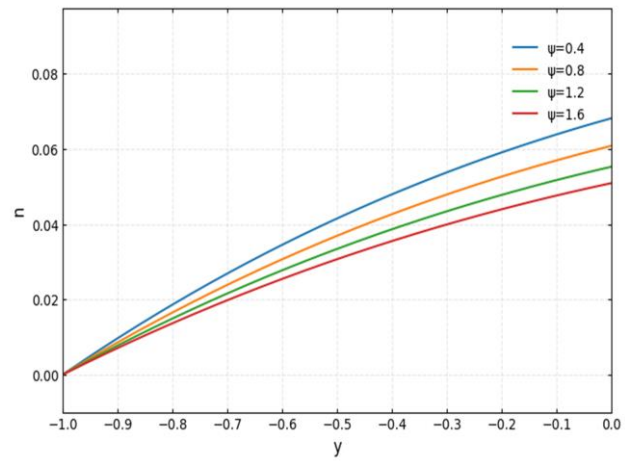

Fig. 38. Change of angular momentum with respect to dimensionless concentration ratio (ψ).

The concentration profiles illustrated in Figs. 39–45 indicate that, except for frequency parameters (ω, η), which produce more significant alterations, many parameters exert only a neg-

ligible influence on species concentration. An insignificant reduction in concentration occurs with an increase in Reynolds number (R) and material parameter (k), suggesting a marginal enhancement in mixing and heat transfer.

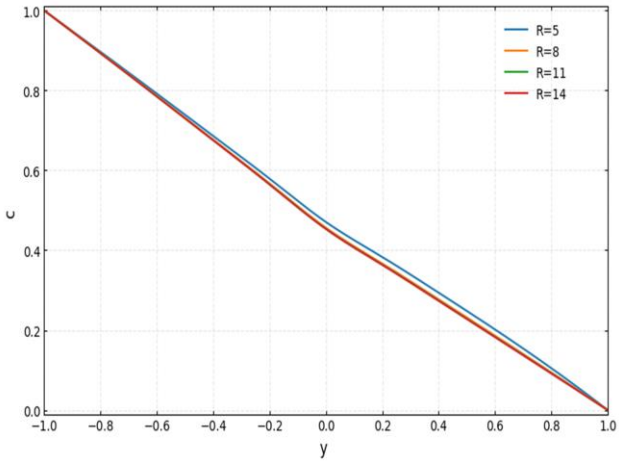

Fig. 39. Change of diffusion with respect to Reynolds number (R).

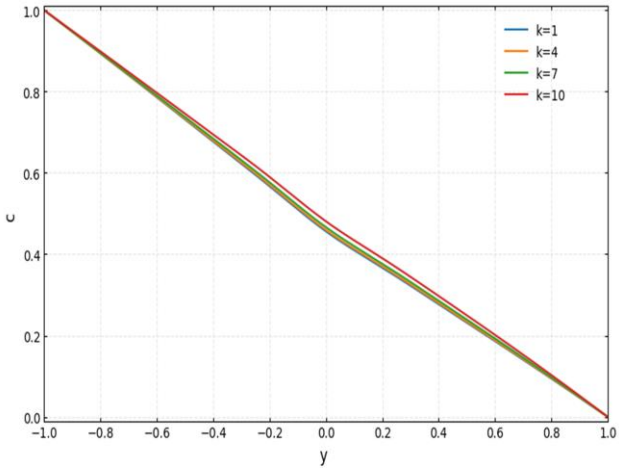

Fig. 40. Change of diffusion with respect to material parameter (k).

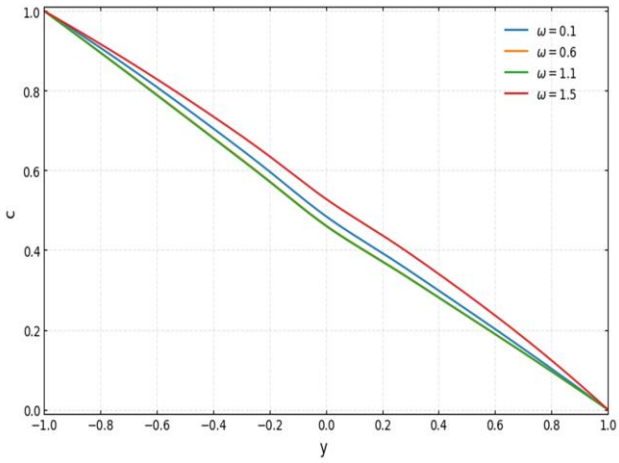

Fig. 41. Change of diffusion with respect to non-uniform temperature amplitude (ω).

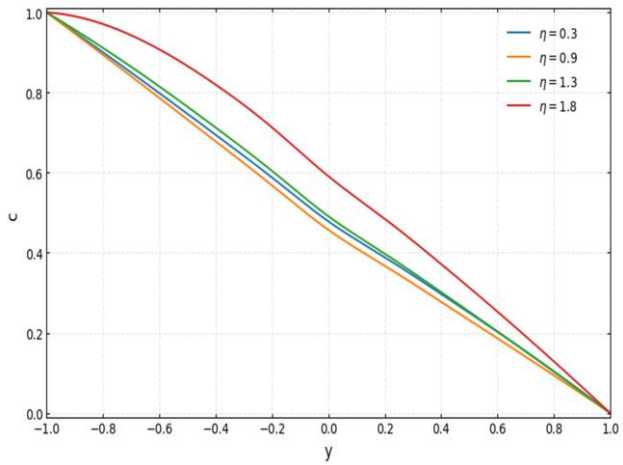

Fig. 42. Change of diffusion with respect to non-uniform temperature amplitude (η).

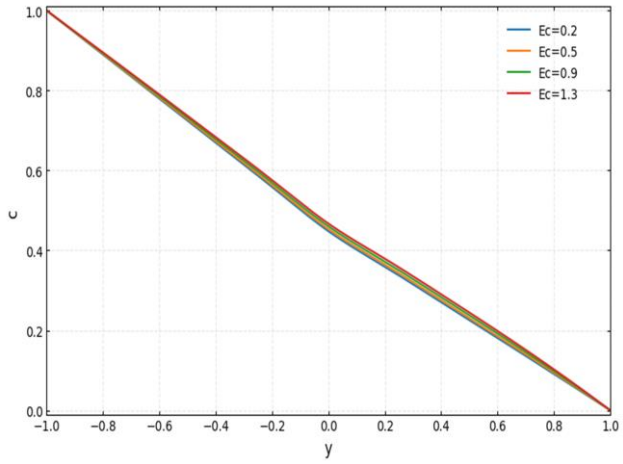

Fig. 43. Change of diffusion with respect to Eckert number (Ec).

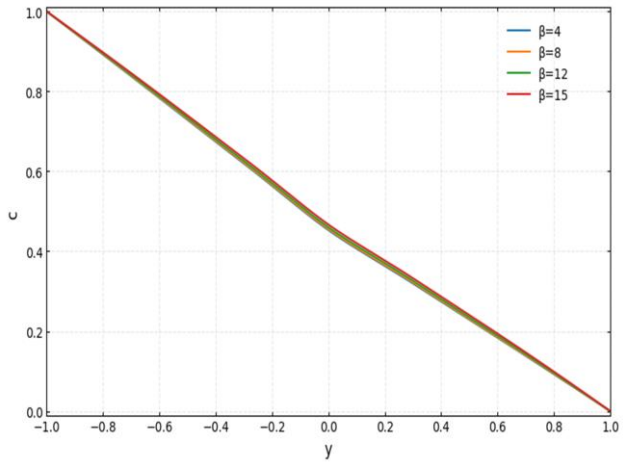

Fig. 44. Change of diffusion with respect to variable thermal conductivity (β).

The increased η significantly elevates concentration in certain areas of the domain due to enhanced thermal non-uniformity, facilitating mass transfer, while the elevated ω marginally raises concentration near the left border. In this context, vis-

cous heating and its related effects exert a minimal impact on concentration, as seen by the insignificant influence of the β parameter and Eckert number (Ec). For all values of the velocity slip parameter $\mu\xi$, the value of c decreases steadily from left to right without much difference between the curves. This indicates that changing $\mu\xi$ has almost no effect on diffusion over the entire domain. The distribution can be substantially altered by η and ω, while other factors induce only minor variations.

4.2. Analysis of the heat transfer rate

The non-dimensional transfer rates on the boundaries obtained using Eq. (20) are presented in the form of bar charts. Figures 46a and 46b depict the variations of Nusselt number for various pertinent parameters. It is very clear that the rate of transfer on both boundaries is largely influenced by these parameters, particularly in the presence of magnetic fields, heat loss, temperature and concentration fluctuations. According to the variations in the Nusselt number, for most parameters, Nu_1 and Nu_2 move in opposition to one another, which means that Nu_1 decreases and Nu_2 increases. The thermal and buoyancy factors (Gr), (Gc), and (M) have a significant impact on enhancing heat transmission, as seen in Fig. 46a, with Nu_2 displaying large positive peaks. Figure 46b demonstrates that the most significant parameter is always Nu_2, while slip and thermal conductivity parameters have a minimal impact on convective heat transfer. This indicates that in these circumstances, thermal performance is improved.

According to the shear stress profiles, for most parameters, both st_1 and st_2 exhibit negative trends. In other words, the flow zone has an increased wall resistance. Shear stress behaviour is influenced by buoyancy and magnetic factors, as seen by changes in wall drag intensity in Fig. 47a. The distribution of shear stress is altered by permeability and slip parameters, as seen in Fig. 47b. Wall friction tends to decrease with increasing slip conditions, allowing fluid to flow more easily close to the edges.

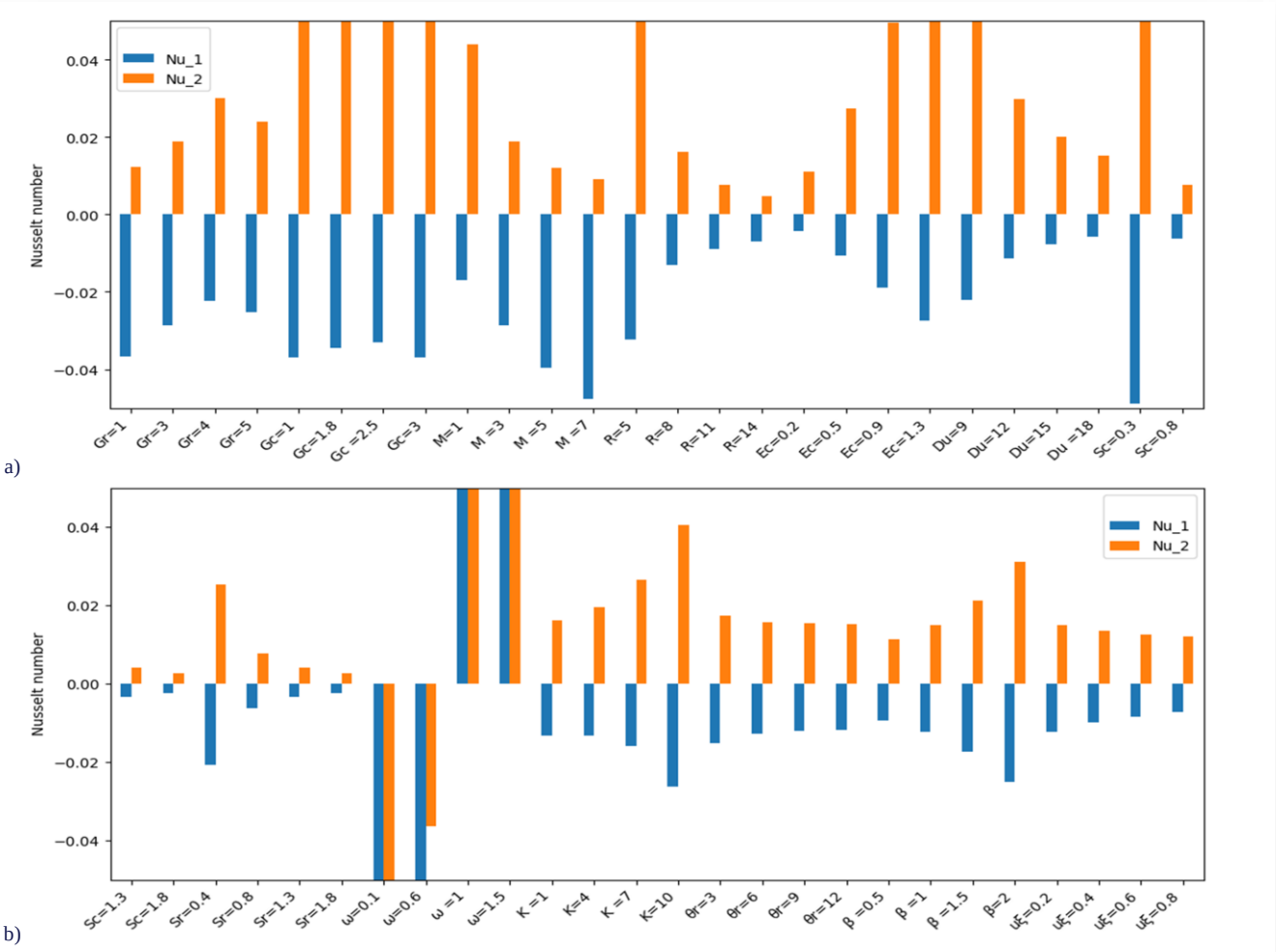

Fig. 46. Nusselt number variations for different parameters.

The Sherwood number distributions demonstrate that Sh_1 and Sh_2 remain almost constant with relatively minor variations across all values. This implies that the features of mass transmission remain unchanged. Buoyancy and magnetic-related parameters have a minor impact on concentration gradients in Fig. 48a, which implies that they have a minor impact on diffusion rates. Small variations in Sherwood numbers are caused by permeability and slip effects, as seen in Fig. 48b. Consequently, there is a little reduction in mass transfer at the channel walls due to improved slip conditions.

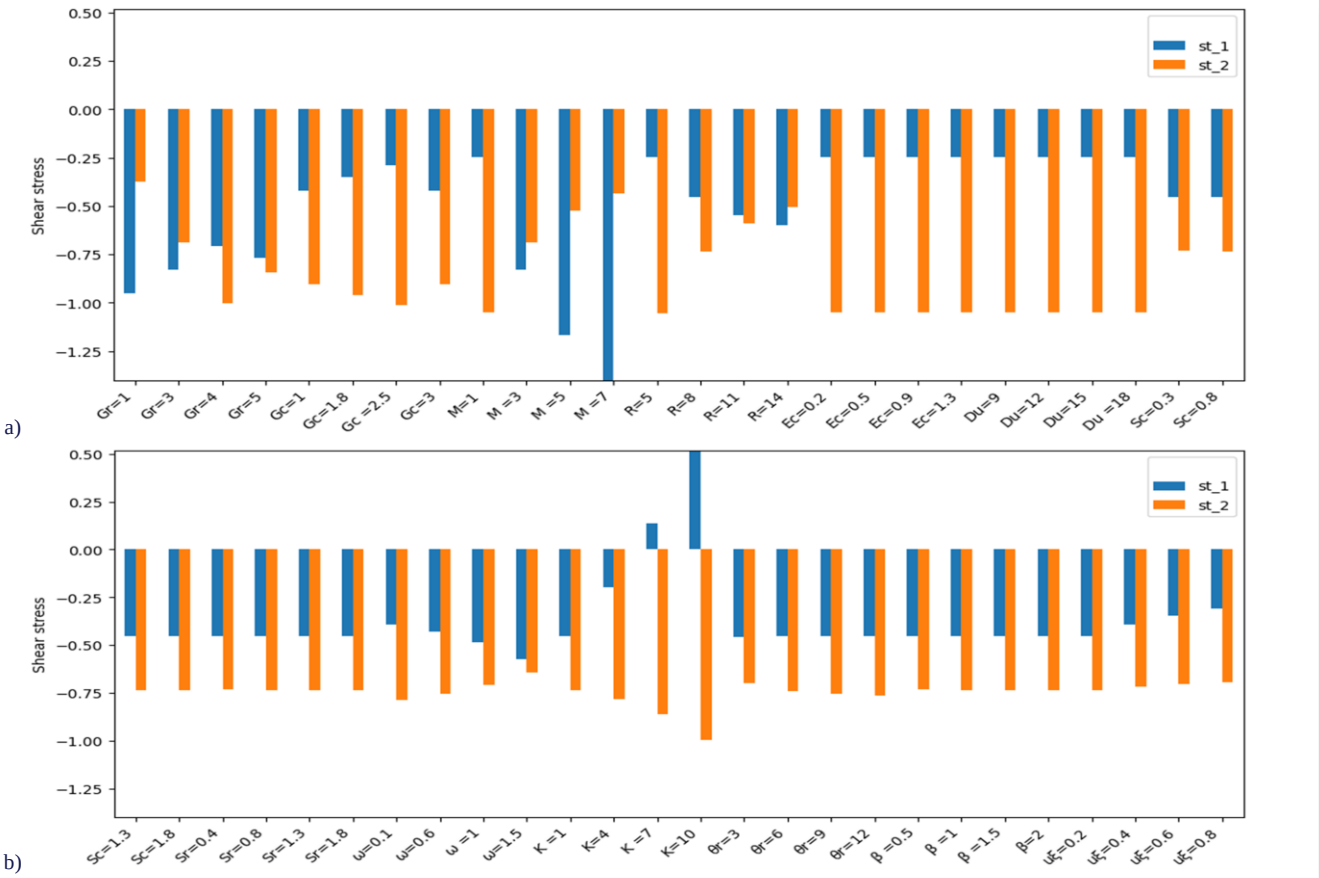

Fig. 47. Shear stress number variations for different parameters.

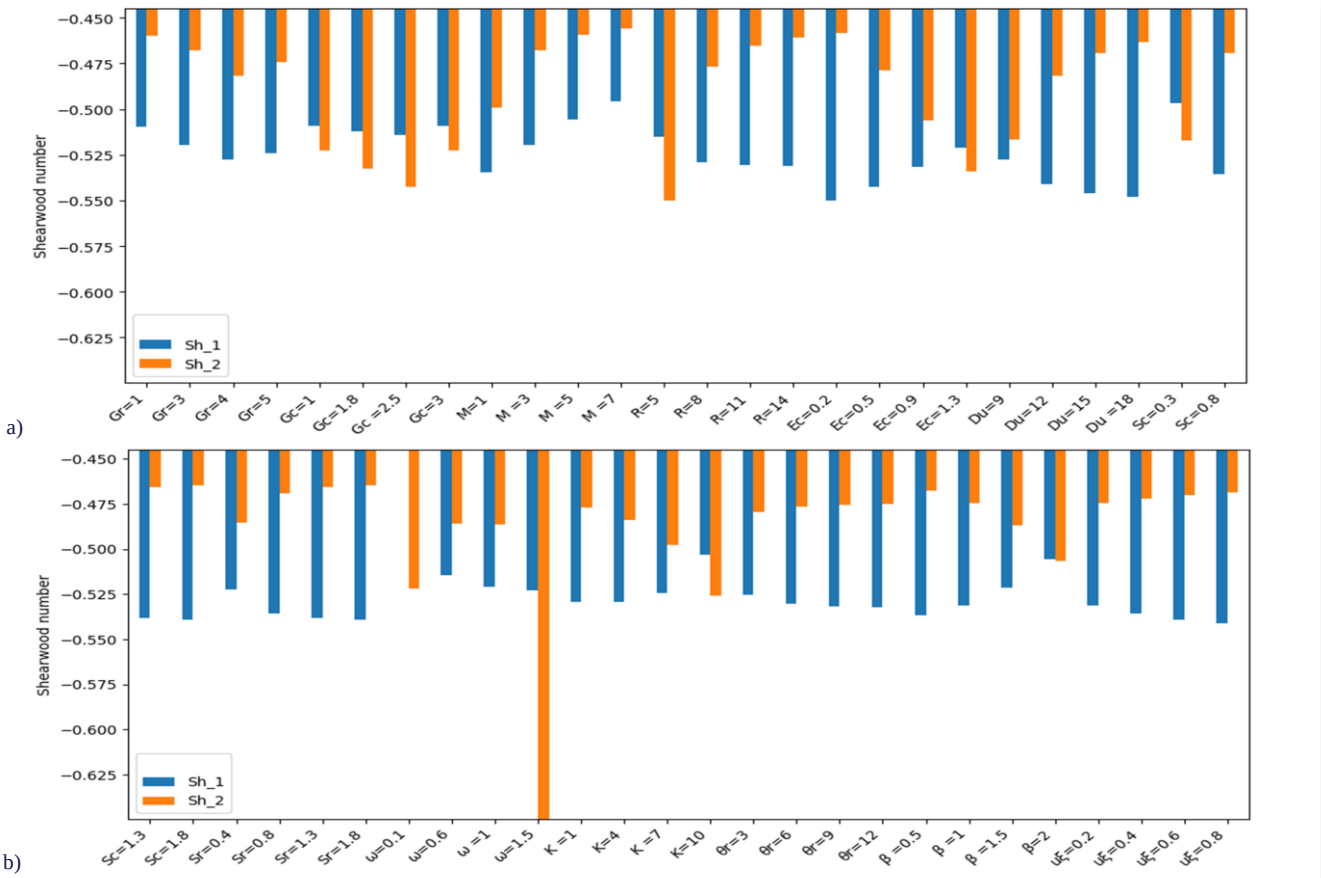

Fig. 48. Shearwood number variations for different parameters.

4.3. Analysis of entropy values

The entropy values obtained using Eq. (21) are presented in Table 1. Entropy study indicates that the molecular Grashof number (Gc) results in a gradual reduction of entropy, while the Grashof number (Gr) leads to an increase. The material parameter (k) significantly reduces entropy formation, signifying enhanced thermal efficiency, whereas the magnetic field strength (M) elevates it due to the Lorentz force effects. At elevated values, the Dufour number (Du) leads to an increased entropy, but the Reynolds number (R) shows minimal fluctuations. The Soret number (Sr) marginally elevates the entropy, whereas the Schmidt number (Sc) significantly diminishes it. The frequency parameter (ω) exhibits a non-monotonic trend, with the entropy increasing under certain situations and decreasing under others. The dimensionless concentration ratio (ψ) markedly decreases the entropy, whereas the velocity slip parameter ($\mu\xi$) shows minimal alteration. The variable viscosity parameter (θ_r) and variable thermal conductivity parameter (β) exert a minimal influence. Entropy generation is typically augmented by Gr, M and Du, whereas it is mitigated by elevated k, Sc and ψ.

Table 1. Generated entropy values.

Parameter	Entropy	Parameter	Entropy	Parameter	Entropy
Gr = 1	5.05726	Du = 9	4.859	θ_r = 3	4.90557
Gr = 3	5.28402	Du = 12	5.00979	θ_r = 6	4.96241
Gr = 4	5.37617	Du = 15	5.06475	θ_r = 9	4.97643
Gr = 5	5.34659	Du = 18	5.09302	θ_r = 12	4.98265
Gc = 1	4.86612	Sc = 0.3	7.74489	β = 0.5	5.01018
Gc = 1.8	4.83861	Sc = 0.8	3.20877	β = 1	4.96761
Gc = 2.5	4.7892	Sc = 1.3	2.068	β = 1.5	4.89166
Gc = 3	4.86612	Sc = 1.8	1.55738	β = 2	4.78118
M = 1	4.93146	Sr = 0.4	4.90236	Ω = 0.2	4.9681
M = 3	5.28402	Sr = 0.8	5.00063	Ω = 0.4	4.96736
M = 5	5.38571	Sr = 1.3	5.02133	Ω = 0.6	4.96712
M = 7	5.83279	Sr = 1.8	5.02894	Ω = 0.8	4.96699
R = 5	4.7392	ω = 0.1	6.03763	ψ = 0.4	7.63652
R = 8	4.95292	ω = 0.6	5.11414	ψ = 0.8	2.07629
R = 11	4.89488	ω = 1	5.06474	ψ = 1.2	1.04662
R = 14	4.82817	ω = 1.5	5.65689	ψ = 1.6	0.686233
Ec = 0.2	4.93593	K = 1	4.95292	$\mu\xi$ = 0.2	4.96761
Ec = 0.5	4.9332	K = 4	4.70198	$\mu\xi$ = 0.4	4.97675
Ec = 0.9	4.93121	K = 7	4.04358	$\mu\xi$ = 0.6	4.97886
Ec = 1.3	4.93157	K = 10	0.549262	$\mu\xi$ = 0.8	4.97759

4.4. Validation section

The non-dimensional system of equations was solved by the Runge-Kutta method under the ND Solve technique in the Mathematica package. The numerical computations were performed up to the accuracy of 10^{-5}. The variations of velocity, angular velocity, temperature and diffusion were validated with the studies of Kumaraswamy et al. [8], Gosty et al. [16], Suresh et al. [19], and found to be in good agreement.

5. Conclusions

The impact of various physical parameters on the entropy generation, heat and mass transfer in a vertical channel with immiscible fluids and non-uniform thermal distribution with slip effects is examined in this thorough investigation.

- The findings show that the transfer of momentum, thermal energy and solute concentrations under various circumstances exhibit consistent behaviour.
- It is confirmed that buoyancy forces (via increasing Gr and Gc) greatly improve heat/mass transfer and velocity profiles while simultaneously decreasing the angular velocity, demonstrating the stabilising function of strong convective flows. The distribution of shear stress is also significantly influenced by these parameters, indicating the development of two-layered boundary structures with opposing near-wall and far-field velocity gradients.
- It is shown that Reynolds number (R) and magnetic field strength (M) are the main damping factors for angular motion and velocity. While M prevents flow through magnetic resistance, R enhances momentum transfer while reducing rotational persistence. Their influence is especially apparent in shear stress and entropy formation, indicating their critical function in energy dissipation.
- The Nusselt number, which measures heat transfer trends, exhibits asymmetrical behaviour across surfaces. While Nu_2 turns positive under high ω, η, or Ec, indicating dominant outward heat flux in dynamic or dissipative regimes, persistently negative Nu_1 values suggest backward diffusion or surface absorption. This emphasises how rotational effects and porous media can improve heat transfer away from the core domain.
- On the other hand, diffusion-driven solute absorption is reflected in mass transfer (Sherwood numbers), which is mostly negative and constant. The fact that Du and Sr have little effect on Sh values indicates that mass transfer is more dependent on molecular diffusion and boundary layer thickness and less susceptible to dynamic forces.
- The system exhibits notable irreversibility trends, as revealed by the entropy analysis. While parameters like M, R and k increase entropy generation, indicating their dissipative influence, Gr and Gc help to lower entropy, exhibiting organised flow behaviour. It is interesting to note that Ec and Du show secondary and nonlinear effects, while β and Ω contribute relatively little. This implies that system-scale fluid dynamics, as opposed to localised diffusion mechanisms, control the entropy.
- Higher Nusselt numbers indicate that buoyancy, magnetic and slide phenomena all improve heat transfer. Shear stress decreases as slip and permeability increase. Wall friction decreases as a result. Mass transfer is stable under all conditions since Sherwood number variations are still quite tiny.
- Limitations of the work: The limitations of the work are the steady-state assumption, constant thermo-physical properties and simplified interfacial conditions.

- Future work: The present work can be extended to transient and time-dependent analysis on different geometries.

References

[1] Fatima, N., Nisar, K.S., Shaheen, S., Arain, M.B., Ijaz, N., & Muhammad, T. (2023). A case study for heat and mass transfer of viscous fluid flow in double layer due to ciliated channel. *Case Studies in Thermal Engineering*, 45, 102943. doi: 10.1016/j.csite.2023.102943

[2] Reddy, M.V., Meenakumari, R., Sucharitha, G., Ali, F., Zafar, S.S., & Lakshminarayana, P. (2024). Heat and mass transfer analysis of conducting non-Newtonian nanofluid flows over an elongating sheet with a non-uniform heat source. *Modern Physics Letters B*, 38(35), 2450349. doi: 10.1142/s0217984924503494

[3] Srinivasulu, T., & Goud, B.S. (2021). Effect of inclined magnetic field on flow, heat and mass transfer of Williamson nanofluid over a stretching sheet. *Case Studies in Thermal Engineering*, 23, 00819. doi: 10.1016/j.csite.2020.100819

[4] Govindarajan, A.G., Sasikumar, J., & Vaidehi, P. (2022). Heat and mass transfer effect on unsteady flow of two stratified immiscible fluids with thermal radiation. *2nd International Conference on Mathematical Techniques and Applications*, 24–26 March, Kattankulathur, India. *AIP Conference Proceedings* 2516(1), 170013. doi: 10.1063/5.0109222

[5] Rabha, R., & Deka, R. (2024). Heat And Mass Transfer on Flow Past an Accelerated Plate Through Porous Medium with Variable Temperature and Mass Diffusion in Presence of Heat Source/Sink. *East European Journal of Physics*, 1, 269−277. doi: 10.26565/2312-4334-2024-1-23

[6] Nurni, V.N., Ballal, B.N., Ghosh, S., & Vaughan, J. (2024). Heat, Mass, Momentum and Charge Transport. In *Treatise on Process Metallurgy. Volume 1: Process Fundamentals* (pp. 565–679). Elsevier. doi: 10.1016/b978-0-323-85935-6.00018-0

[7] Jan, A., Farooq, U., Khan, M.I., & Aslam, F. (2025). Applications of neural networking analysis on drag reduction and heat transfer rate of non-Newtonian fluid flows in energy storage systems. *International Communications in Heat and Mass Transfer*, 169, 109569. doi: 10.1016/j.icheatmasstransfer.2025.109569

[8] Kumaraswamy, P., Ramakrishna Goud, T., Suresh Babu, B., Gosty, V., Srinivas, G., Haripriya, T., & Makinde, O.D. (2025). Numerical analysis on heat and mass transfer of immiscible fluids in a vertical channel with diffusion effects. *Partial Differential Equations in Applied Mathematics*, 13, 101139. doi: 10.1016/j.padiff.2025.101139

[9] Baithalu, R., Mishra, S.R., Pattnaik, P.K., & Panda, S. (2024). Analysis of heat and mass transfer rates in conducting Casson fluid flow over an expanding surface considering Ohmic heating and Darcy dissipation effects. *Partial Differential Equations in Applied Mathematics*, 12, 100972. doi: 10.1016/j.padiff.2024.100972

[10] Ouedraogo, R.W., Namoano, D., Ilboudo, J.M., Igo, W.S., Sawadogo, G.L., & Ouedraogo, D. (2025). Modeling Heat and Mass Transfer in Laminar Forced Convection in A Vertical Channel: Influence of Inlet Fluid Temperature. *IRA-International Journal of Applied Sciences*, 19(4), 89–106. doi: 10.21013/jas.v19.n4.p1

[11] Kalyan, S., Sharan, A., & Chamkha, A.J. (2023). Heat and mass transfer of two immiscible flows of Jeffrey fluid in a vertical channel. *Heat Transfer*, 52(1), 267−288. doi: 10.1002/htj.22694

[12] Kemparaju, S., Swamy, H.K., Sankar, M., & Mebarek-Oudina, F. (2022). Impact of thermal and solute source-sink combination on thermosolutal convection in a partially active porous annulus. *Physica Scripta*, 97(5), 055206. doi: 10.1088/1402-4896/ac6383

[13] Babu, B.S., Santhosh, K., Kumari, G., & Srinivas, G. (2022). Numerical solution of MHD free convective Jeffrey fluid of variable viscosity with chemical reaction and heat source. *Materials Today: Proceedings*, 66, 2636−2641. doi: 10.1016/j.matpr.2022.07.226

[14] Kandagal, M., & Kempepatil, R. (2024). An investigation of the heat and mass transfer effects in vertical channels with immersible fluid flow through a porous matrix. *Journal of Applied Mathematics and Mechanics*, 104(10). doi: 10.1002/zamm.202300998

[15] Kumar, M.A., Mebarek-Oudina, F., Mangathai, P., Shah, N.A., Vijayabhaskar, C., Venkatesh, N., & Fouad, Y. (2025). The impact of Soret Dufour and radiation on the laminar flow of a rotating liquid past a porous plate via chemical reaction. *Modern Physics Letters B*, 39(10), 2450458. doi: 10.1142/S021798492450458X

[16] Gosty, V., Srinivas, G., & Suresh Babu, B. (2024). Numerical investigation of slip effects on heat and mass transfer in a vertical channel with immiscible micropolar and viscous fluids of variable viscosity. *Heat Transfer*, 53(7), 3987−4012. doi: 10.1002/htj.23120

[17] Gosty, V., Srinivas, G., Babu, B.S., Goud, B.S., Hendy, A.S., & Ali, M.R. (2024). Influence of variable viscosity and slip on heat and mass transfer of immiscible fluids in a vertical channel. *Case Studies in Thermal Engineering*, 58 doi: 10.1016/j.csite.2024.104368

[18] Umavathi, J.C., & Sheremet, M.A. (2021). Heat transfer of viscous fluid in a vertical channel sandwiched between nanofluid porous zones. *Journal of Thermal Analysis and Calorimetry*, 144(4), 1389–1399. doi: 10.1007/S10973-020-09664-1

[19] Suresh Babu, B., Srinivas, G., & Srikanth, G.V.P.N. (2022). Finite element analysis of diffusion effects on convective heat and the mass transfer of two fluids in a vertical channel. *International Journal of Automotive and Mechanical Engineering*, 14(1), 3998−4012. doi: 10.15282/ijame.14.1.2017.14.0324

[20] Naseem, T., Mebarek-Oudina, F., Vaidya, H., Bibi, N., Ramesh, K., & Khan, S. (2025). Numerical analysis of entropy generation in Joule heated radiative viscous fluid flow over a permeable radially stretching disk. *Computer Modeling in Engineering and Sciences*, 143(1), 351−371. .doi: 10.32604/cmes.2025.063196

[21] Ghasemi, S.E., & Ranjbar, A. (2025). Entropy Generation Study on Natural and Forced Convection of Nanofluid Flow in Vertical Channels. *Engineering Reports*, 7, e13096. doi: 10.1002/eng2.13096

[22] Suresh Babu, B., Srinivas, G., & Srikanth, G.V.P.N. (2018). Finite element study of convective heat and mass transfer of two fluids in a vertical channel of variable width with Soret and Dufour effects. In *Numerical Heat Transfer and Fluid Flow. Lecture Notes in Mechanical Engineering* (pp. 537−546). Singapore: Springer Singapore. doi: 10.1007/978-981-13-1903-7_62

[23] Abdel-wahed, M.S., Ahmed, S.I., Mekheimer, K.S., & Sayed, A.Y. (2024). Entropy generation analysis of a micropolar fluid in a corrugated channel with convective and slip conditions. *Case Studies in Thermal Engineering*, 57 104283. doi: 10.1016/j.csite.2024.104283

[24] Mebarek-Oudina, F., Dharmaiah, G., Prasad, J.R., Vaidya, H., & Kumari, M.A. (2025). Thermal and flow dynamics of magneto-hydrodynamic Burgers' fluid induced by a stretching cylinder with internal heat generation and absorption. *International Journal of Thermofluids*, 25, 100986. doi: 10.1016/j.ijft.2024.100986

[25] Usha, B., & Gireesha, B.J. (2025). Entropy generation analysis of micropolar fluid flow through a vertical microchannel under the combined effect of Joule heating, viscous dissipation, and thermal radiation with convective boundary conditions. *International*

Journal of Modelling and Simulation, 45(6) 1932−1944. doi: 10.1080/02286203.2024.2306088

[26] Kumar, A., & Yadav, P.K. (2023). Entropy generation analysis of non-miscible couple stress and Newtonian fluid in an inclined porous channel with variable flow properties: HAM Analysis. *International Journal of Modern Physics B*, 38(28), 2450390. doi: 10.1142/s0217979224503909

[27] Govindarajulu, K., Reddy, A.S., Jagadeshkumar, K., Srinivas, S., Kumar, B.R., & Vajravelu, K. (2023). Entropy generation on MHD pulsatile flow of third grade hybrid nanofluid in a vertical porous channel with nonuniform heat source/sink, variable viscosity, thermal conductivity, and Joule heating: A numerical study. *Numerical Heat Transfer Part A: Applications*, 85(24), 4184−4203. doi: 10.1080/10407782.2023.2255929

[28] Nayak, M.K., Shaw, S., Ijaz, K.M., Makinde, O.D., Chu, Y.-M., & Khan, S.U. Interfacial layer, and shape effects of modified Hamilton's Crosser model in entropy optimized Darcy-Forchheimer flow. *Alexandria Engineering Journal*, 60(4), 4067−4083, doi: 10.1016/j.aej.2021.02.010

[29] Reddy, C.S., Mahanthesh, B., Rana, P., & Muhammad, T. (2023). Entropy generation and thermal analyses of a Cross fluid flow through an inclined microchannel with non-linear mixed convection. *Journal of Applied Mathematics and Mechanics*, 103(8). doi: 10.1002/zamm.202100364

[30] Yadav, P., Kumar, A., & Filippov, A.N. (2023). Analysis of entropy production of immiscible micropolar and Newtonian fluids flow through a channel: effect of thermal radiation and magnetic field. *Colloid Journal*, 85(1), 101–121. doi: 10.31857/s0023291222700033

[31] Prasad, J.L.R., Mebarek-Oudina, F., Dharmaiah, G., Rao, P.B., & Vaidya, H. (2024). Melting Flow Analyzation of Radiative Riga Plate Two-Phase Nano-Fluid Across Non-Flatness Plane with Chemical Reaction. *Frontiers in Heat and Mass Transfer*, 22(5), 1515−1532. doi: 10.32604/fhmt.2024.057854

[32] Khan, Z.H., Makinde, O.D., Usman, M., Ahmad, R., & Khan, W.A. (2025). Fractional order unsteady mixed convection in porous-filled concentric pipes: Entropy analysis. *Alexandria Engineering Journal*, 129, 483−503. doi: 10.1016/j.aej.2025.06.047

[33] Shamshuddin, M.D., & Ibrahim, W. (2022). Finite element numerical technique for magneto-micropolar nanofluid flow filled with chemically reactive Casson fluid between parallel plates subjected to rotatory system with electrical and Hall currents. *International Journal of Modelling and Simulation*, 42(6), 985−1004. doi: 10.1080/02286203.2021.2012634

[34] Madhuri, N.J.P., Shamshuddin, M.D., & Salawu, S.O. (2025). Exploring radiative heat transfer and buoyancy effects on Tiwari-Das nanofluid flow model in permeable rotating disc: Finite element study. *Thermal Science and Engineering Progress*, 65, 103855. doi: 10.1016/j.tsep.2025.103855

[35] Jan, A., Khan, M.I., Farooq, U., Aslam, F., & Adnan, R. (2026). Response surface method base multi objective analysis of drag reduction and heat transfer rate in magnetized squeezing channel flow with ohmic heating and viscous dissipation. *International Communications in Heat and Mass Transfer*, 170, 110024. doi: 10.1016/j.icheatmasstransfer.2025.110024

[36] Bejan, A. (1995). *Entropy generation minimization. The method of thermodynamic optimization of finite-size systems and finite-time processes* (1st. ed.). Boca Raton, CRC Press. doi: 10.1201/9781482239171